Statistical Mechanics of Superparamagnetic Colloidal Dispersions Under Magnetic Fields

by

Jordi Andreu Segura

PhD Thesis in Materials Science

Departament de Física
Universitat Autònoma de Barcelona

14th January 2013

under the supervision of:

Dr. Jordi Faraudo Gener
Departament de Teoria i Simulació de Materials
Institut de Ciència de Materials de Barcelona

Dr. Juan Camacho Castro
Departament de Física, Grup de Física Estadística
Universitat Autònoma de Barcelona

La present Tesi Doctoral que porta per títol *Statistical Mechanics of Superparamagnetic Colloidal Dispersions Under Magnetic Fields* ha estat realitzada per en JORDI ANDREU SEGURA i desenvolupada al Departament de Teoria i Simulació de Materials de l'Institut de Ciència de Materials de Barcelona i al Departament de Física Estadística de la Universitat Autònoma de Barcelona sota la supervisió del Dr. Jordi Faraudo Gener i el Dr. Juan Camacho Castro, i que per així consti, en dónen fe els sotasignants.

Jordi Andreu Segura

Dr. Jordi Faraudo Gener.
Departament de Teoria i Simulació de Materials,
Institut de Ciència de Materials de Barcelona.

Dr. Juan Camacho Castro.
Departament de Física Estadística,
Universitat Autònoma de Barcelona.

A Bellaterra, 14 de gener de 2013.

Agraïments

Al llarg de la nostra vida, diversa gent ens acompanya compartint, doncs, aquest camí. Per a ells i elles, amb els i les que he estat caminant durant aquests anys, van dirigides aquestes paraules d'agraïment.

Primerament, al Dr. Juan Camacho i el Dr. Jordi Faraudo, els directors d'aquest treball de Tesi i amb els que he tingut el plaer de treballar, aprendre i gaudir durant aquests últims anys. Sense ells, la seva empenta, atenció, criteri, i la confiança dipositada en mi des del primer dia, el resultat d'aquesta tesi no hauria estat el que, ara, ja és. També agrair la confiança mostrada per el Dr. Lluís Miquel Martínez i la Dra. Maria Benelmekki, amb els que he tingut el plaer de col·laborar de forma estreta i als que també agraeixo la seva implicació en aquest treball, aportant noves idees i punts de vista.

En un ambit més personal, voldria també agrair a tots el meus companys i companyes de l'Institut de Ciència de Materials de Barcelona i del Deparatment de Física de la Universitat Autònoma de Barcelona, que heu estat uns quants! Als companys de despatx, als tècnics i personal de suport, administració, etc... no faré una llista exhaustiva, em deixaria a algú de forma immerescuda, segur. Gràcies per l'ambient de treball del que m'heu fet gaudir durant aquests anys. Ha estat immillorable, sens dubte!

Als amics i amigues de tota la vida, perquè amb el vostre suport i ànims m'heu ajudat a disfrutar encara més aquest treball, i de moltes altres coses!

I, obviament, a la meva familia, als meus germans, cunyat i cunyades... i a la mare. Sempre heu estat al meu costat, animant-me a continuar amb allò que m'ha fet feliç.

A tots vosaltres, moltes gràcies.

Contents

1 Introduction 3
1.1 Superparamagnetism . . . 3
1.1.1 Relaxation mechanisms . . . 4
1.1.2 Magnetization at thermal equilibrium . . . 7
1.1.3 Superparamagnetic nanoparticles . . . 9
1.1.4 Applications . . . 10
1.2 Magnetic Colloidal Dispersions . . . 13
1.2.1 Stability . . . 14
1.2.2 Structure formation under magnetic fields . . . 19
1.2.3 Aggregation kinetics . . . 23
1.3 Magnetophoresis . . . 24
1.3.1 Magnetic separation . . . 25
1.3.2 High Gradient Magnetic Separation: inhomogeneous conditions . 27
1.3.3 Precision Magnetic Separation: homogeneous conditions . . . 28
1.3.4 Microfluidics Separation Devices . . . 30
1.4 Simulation Techniques . . . 32
1.5 Motivation & Scope . . . 35

2 Results I: Chain formation under uniform magnetic fields 37
2.1 Objectives . . . 37
2.2 Summary . . . 38
2.3 Results . . . 38
2.3.1 Aggregation kinetics and equilibrium state . . . 38
2.3.2 Irreversible chain growth . . . 43
2.4 Conclusions . . . 47

3 Results II: Magnetophoresis 49
3.1 Objectives . . . 49
3.2 Summary . . . 50
3.3 Results . . . 51
3.3.1 Magnetophoretic separation under homogeneous conditions . . . 51
3.3.2 Separator design . . . 54
3.3.3 Mixtures of magnetic and non-magnetic particles . . . 55
3.4 Conclusions . . . 58

4 Conclusions & Perspectives **61**
4.1 Conclusions 61
4.2 Perspectives 63

5 Articles **65**
5.1 Article 1 67
5.2 Article 2 79
5.3 Article 3 93
5.4 Article 4 109
5.5 Article 5 121

List of Figures

1 Evolution of the number of articles in peer-reviewed journals during the last 20 years involving magnetic particles's synthesis and magnetic separation technology (**source:** Thomson Reuters, Web Of Knowledge). In parenthesis, we also show the number of related U.S. patents published during the same period of time (**source:** United States Patent and Trademark Office, http://www.uspto.gov) [last update: 30th October 2012]. 2

1.1 Schematic representation of the change on the coercitivity field H_{C} as a function of particle size. The maximum of the coercitivity field corresponds to the critical D_{C} size of the material, a situation in which a magnetic particle consists of a single magnetic domain. For smaller particles, the transition to the superparamagnetic state D_{SP} appears when the thermal energy suffices to flip the magnetization state, overcoming the anisotropic energy barrier, a situation corresponding to zero coercitivity field and zero magnetic remanence. 4

1.2 Magnetization loop obtained with a *Superconducting Quantum Interference Device* (SQUID) magnetometer at $T = 298$K (circles) and $T = 5$K (squares) for Fe_2O_3 nanoparticles of 5nm in size. The upper inset shows the *Zero-Field Cooling, Field Cooling* (ZFC-FC) curves used to determine the blocking temperature T_B of the sample. The lower inset shows a closer view of the magnetization curve at $T = 5$K, where a certain remanence is observed. 6

1.3 Magnetization curve for the 12 nm γ-Fe_2O_3 nanocrystals. Symbols are experimental data obtained from SQUID magnetometer measurements at 298K and the solid line is the corresponding fit to a Langevin function according to Eqs. 1.5 and 1.6. 8

1.4 Different strategies can be adopted in the design of composite superparamagnetic colloidal particles. A first approach namely *core-shell* is the coating of a magnetic core formed by some superparamagnetic particles with some non-magnetic layer. A second approach namely *matrix-dye* consists of embedding superparamagnetic nanoparticles in a non-magnetic porous matrix. 10

1.5 Magnetic nanoparticles are often decorated onto their surfaces with specific ligands or chemical groups (sometimes with more than one at a time) which confer specific functionalities required in different applications. 12

1.6 Schematic plot of the typical potential energy landscape close to the surface of a colloidal particle stabilized through two different strategies: *electrostatic stabilization* (**left**) and *steric stabilization* (**right**). In the first approach, the surface of the particles are coated with charged molecules or groups, conferring a net surface charge to the particles. In this situation, the energy barrier can be adjusted by varying the properties of the solvent. A second strategy is to cover the surface of the particle with large molecules, avoiding the particles to get close enough and overcome the van der Waals attraction at short distances. 15

1.7 Scheme representing the interaction between superparamagnetic particles in different situations with $H_0 < H_1 < H_2$. **a)** Under the effects of an applied magnetic field ($\mathrm{H_0}$), dipolar particles will tend to align along the magnetic field direction with an interaction magnetic energy given by Eq. 1.9. **b)** If the magnetic field is strong enough ($\mathrm{H_1}$), these magnetic particles will align head-to-tail, forming chain-like structures. **c)** The structures formed will become more stable for higher magnetic fields ($\mathrm{H_2}$). 16

1.8 **Left:** Scheme showing a secondary minimum in the energy landscape of a magnetic particle due to the magnetic anisotropic energy contribution. The reversible chaining process between superparamagnetic colloids under the effects of an external magnetic field is related to the existence of this secondary minimum. **Right:** Interaction potential at short distances between two superparamagnetic particles of radius 100 nm and different values for the magnetic strength. The potential energy is calculated as the sum of the attractive van der Waals interactions, the repulsive electrostatic interactions according to the DLVO theory and the potential magnetic energy between particles (Eq .1.9). 18

1.9 Different real structures found in suspensions of superparamagnetic particles. **Left:** Chains formed in a suspension of $\pi_0 = 0\ 023$ and field strengh $\lambda = 19\ 5$. **Center:** Bundles obtained for a suspension with volume fraction $\pi_0 = 0\ 005$ and field strength $\lambda = 37$, with an pulsed magnetic field at frequency $\nu = 2$Hz. **Right:** Fibrous structure under a field strength of $\lambda = 285$ and high concetration ($\pi_0 = 0\ 69$). 20

1.10 Sketch representing different structures observed in the suspension as a function of dipolar interaction parameter Γ and volume fraction. 21

1.11 Example of complex structures obtained in mixtures of particles with different size and magnetic response induced by homogeneous magnetic fields. The fluorescent images show the structure formation in four-component colloidal-particle aqueous suspensions consisting of **a)** ferrofluids, non-magnetic particles (red 0.21 mm and green 1.0 mm) and paramagnetic core particles 2.7 mm. **b)** ferrofluid, 1.0 mm non-magnetic particles (red), 2.7 mm paramagnetic core particles and 9.9 mm non-magnetic particles (green). Each panel includes a sketch of the assembled structure and a magnified view of one of the assembled structures (inset). Scale bars, 20 mm. 22

1.12 Real time-lapse images of the magnetic separation of Chlorella sp. by using 1000 mg L^{-1} TODA nanorods-PDDA by a NdFeB permanent magnet. 26

1.13 Sketch of a *High Gradient Magnetic Separation* device. The fluid containing the target magnetic particles is passed through the magnetized mesh (in red), which retains the magnetic particles of interest. After the separation is accomplished, the magnetic field is removed and the magnetic column is washed in order to recover the magnetic particles captured. 27

1.14 Sketch of the top and bottom view of the *Precision Magnetic Separation* device by SEPMAG Tecnologies S.L. **Left:** Initially, the homogeneous dispersion containing the magnetic particles is placed in the cylindrical cavity of the separator. **Right:** At the end of the separation, all the magnetic particles are accumulated at the walls of the containing vessel and the clean solution can be easily removed. The separation process is monitored by measuring the transmitted light through the sample by a photodetector. 29

1.15 Sketch of a typical nanofluidic device. The standard strategy in nanofluidic devices is the deflection of the trajectories of the particles by generating a magnetic field gradient inside the microfluidic channel perpendicular to the fluid direction. 31

1.16 Diagram showing the different simulation and computational techniques according to the relevant length and time scales of the processes which they can describe. 32

2.1 Time evolution of the average chain length N in Langevin Simulations with different values of Γ and different concentrations. Dashed lines indicate the average chain length N reached at equilibrium, calculated by averaging over the last 0.5 s of each simulation. This figure summarizes the simulation results shown in figures 2 and 3 from article 1. 39

2.2 Average number of particles in a chain $< N >$ in the equilibrium state of superparamagnetic colloids under a strong field as obtained from simulations at different values of the aggregation parameter N^* defined by Eq.2.2. The simulations correspond to different values of the magnetic coupling parameter Γ and the volume fraction π_0. The predicted no aggregation ($N^* \leq 1$) and aggregation ($N^* > 1$) regimes are indicated. The solid line corresponds to the prediction of Eq. 2.2 for the equilibrium size of chains in the aggregation regime (results adapted from article 1). 41

2.3 Time evolution of the average length of chains in simulations with concentration $\sim 0\ 5$ gL^{-1} ($\pi_0 = 5\ 23 \times 10^{-4}$) and magnetic strength parameter $\Gamma = 15$ and 40. The dashed line corresponds to a power-law fit of the form $N \sim t^z$ for the case of $\Gamma = 40$. Figure extracted from article1, figure 1. 42

2.4 **(a)** In Langevin Dynamics simulations, the motion of each individual colloid is calculated at each timestep and the stability of the chain results from the dipolar interactions between colloids in the chain. **(b)** In the Coarse-Grain approach, the motion of each coarse-grain object is calculated through the diffusion coefficients of the anisotropic model ($D^{\perp}$ and $D^{\|}$), rather than through the motion of each individual particle forming the chain. **(c)** 2D-map corresponding to the interaction energy between an incoming test dipolar particle and a chain-like aggregate formed by five colloids with magnetic strength parameter of $\Gamma = 40$. The black dashed line limits the region where $E \leq -k_B T$ and the blue region is the excluded volume, not accessible by other colloids. **(d)** Sketch of the interaction model implemented in our code. Each CG object has two attraction zones, modeled as a sphere of radius r_a tangent to the edge of the aggregate. Any object entering into these zones will immediately aggregate forming a longer chain. This figure has been adapted from figure 1 in article 2. 44

2.5 Time evolution of the average chain length $N(t)$. Comparison between the results obtained from Langevin Dynamics simulations (solid symbols) and Coarse-Grain simulations (open symbols) for the two different systems studied. Circles correspond to case $\Gamma = 40$ $\pi_0 = 5\ 23 \times 10^{-4}$ and squares to case $\Gamma = 247$ $\pi_0 = 4\ 64 \times 10^{-6}$. This plot corresponds to figure 4 in article 2. 46

2.6 Evolution of the relaxation rate $1/\mathrm{T}_2$ of water protons in four dispersions characterized by $\Gamma = 247$ and containing different concentrations of superparamagnetic colloids $\pi_0^{(00)} = 1\ 16 \times 10^{-6} = 8\pi_0^{(03)} = 4\pi_0^{(02)} = 2\pi_0^{(01)}$. Solid lines correspond to the predictions obtained from Coarse-Grain simulations and symbols correspond to experimental data. These results correspond to figure 11 in article 2. 47

3.1 Kinetics of magnetophoretic separation of a 10 gL^{-1} dispersion of superparamagnetic γ-$\mathrm{Fe}_2\mathrm{O}_3$ colloids (sample S1). Symbols correspond to the experimental data under 30 T/m (circles) and 60 T/m (squares) and solid lines are the predictions from the analytical model. The dashed line for the 30 T/m case corresponds to the particle tracers simulations. Figure obtained from results presented in articles 3 and 4. 52

3.2 Comparison between the experimental results (symbols) obtained from the separation of a 1 gL^{-1} dispersion of commercial Estapor® M1-020/50 particles using the 30 T/m separator and the predictions by the analytical model (dashed line). The velocity of a single particle in saturation has been estimated by using the values presented in Tab. 3.1, giving $v_s \approx 4\ 0 \times 10^{-6}$ m/s. The solid line (red) is a fit of the initial decay, leaving the magnetophoretic velocity as a fitting parameter. The value for the magnetophoretic velocity obtained from this fit is $v_s \approx 2\ 6 \times 10^{-4}$ m/s, which greatly exceeds the predicted value for a single colloidal particle. This figure corresponds to figure 3 from article 3. 53

3.3 Snapshots corresponding to the separation process of a superparamagnetic dispersion of particles (sample S1) at different times ($t_0 = 0$ s, $t_1 = 1 \times 10^5$ s, $t_2 = 2 \times 10^5$ s and $t_3 = 5 \times 10^5$ s). The dark circular areas indicate the location of the magnets. The different figures correspond to simulations in open-type (top row) and close-type (bottom row) geometries, and show how the close-type geometry offers a much more homogeneous and faster separation than the open-type one. The magnetic field and the corresponding magnetic gradient obtained for both configurations are shown in figures 1 and 3 from article 4 and this figure has been adapted from figure 4 from article 4. 55

3.4 Magnetophoretic behavior of a mixture of latex particles (red/pink color) and a SDS-NPs suspension under a 60 T/m gradient. (A) After 30 minutes inside the magnetic system, a red/pink spot appears at the center of the vessel, indicating the beginning of latex particles migration to the center of the bottle. (B) After 3 hours, brown-yellow spots appear close to the walls of the vessel confirming the continuous arrival of the SDS-NPs to the walls and the central red spot size increases slightly. (C1 and C2) After 6 hours, the latex particles ring is formed. A clear depletion of the latex particles both near the walls and also at the center of the system is observed. This picture corresponds to figure 4 from article 5. 56

3.5 Snapshots from the 2D-simulations of the magnetophoresis of an aqueous dispersion of γ-Fe_2O_3 superparamagnetic nanoparticles (grey) and latex polystyrene particles (orange) under a magnetic gradient of 30 T/m at different times. Original snapshots in figure 6 from article 4. 58

List of Tables

1.1 Examples of different superparamagnetic particles designed to target specific applications, covering a wide range of sizes, coatings and magnetic saturation values. Typically, the character @ is used to differentiate the core (or dye) composition and the shell (or matrix) nature. 11

2.1 Comparison of the performance between Langevin Dynamics and the Coarse-Grain model proposed for different systems. The Δt is the timestep used in each integration scheme and t_f is the total simulated time. We have also indicated the total amount of CPU cost for each single run, calculated as the number of cores used multiplied by the total elapsed time. In all our calculations we have used a 8-Core AMD Opteron Magny-Cours 6136 processor. Table adapted from table 2 in article 2. 46

3.1 Diameter, overall density and magnetic moment for the colloidal particles reported in article 4. The last two columns are the magnetic strength and the aggregation parameter calculated from particle properties under the experimental conditions of interest. This table summarizes the values supplied in article 3, table 1. 52

a la meva mare i germans,

Preface

The aim of this thesis has been the study of dispersions of superparamagnetic colloidal particles under the effects of uniform and non-uniform magnetic fields. The research project arisen in September 2009, as a private/public collaboration among the Institut de Ciència de Materials de Barcelona (ICMAB-CSIC), the Universitat Autònoma de Barcelona (UAB) and SEPMAG Tecnologies S.L., in the framework of the national TRACE program (PET2008-0281) and aimed to enhance the transfer of new knowledge between basic scientific research and technological companies. The main goal of this collaboration project was the understanding of the physical mechanisms behind the fast magnetic separation of magnetic colloidal particles in solution, as an emerging technology with different potential applications.

Magnetic nanoparticles and their applications in a wide range of different fields have become an interesting research area from the scientific and also the technological points of view. This is reflected in the vast number of scientific papers in peer review journals, research groups and brand new launched companies that appeared during the last 20 years, which have focused their attention on the development of new nanotechnological applications involving magnetic particles (see Fig. 1). The scope of these applications is rather broad, from waste-water treatment to new clinical applications and immunoassays. In spite of the large number of new patents published worldwide and new applications already available at industrial scale, a good understanding of the basic mechanisms behind the behavior of dispersions of magnetic nanoparticles is still missing. Therefore, the transition from phenomenological descriptions to theoretical tools would be very useful to improve the rational design of such processes and technologies.

This thesis dissertation has been structured fulfilling the requirements to obtain the PhD in Materials Science by the Universitat Autònoma de Barcelona. In the first chapter we provide the fundamental concepts and the context related with the work developed. We review the concepts of superparamagnetism, colloidal suspensions and their stability, aggregation structures and kinetics, magnetophoresis, and of the basic simulation tools employed. In the second and third chapters we present a summary of the results obtained and published in peer-reviewed journals, and accepted by the doctoral commission. The fourth chapter summarizes the main conclusions related to the different topics covered along this thesis, as well as some open questions and future

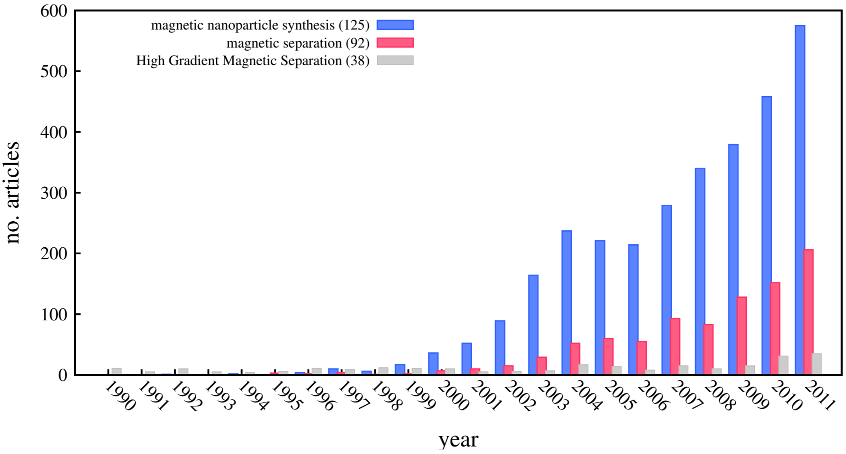

Figure 1: Evolution of the number of articles in peer-reviewed journals during the last 20 years involving magnetic particles s synthesis and magnetic separation technology (**source:** Thomson Reuters, Web Of Knowledge). In parenthesis, we also show the number of related U.S. patents published during the same period of time (**source:** United States Patent and Trademark Office, http://www.uspto.gov) [last update: 30th October 2012].

perspectives. The original articles forming part of this dissertation and accepted by the doctoral commission have been appended at the end of the present document.

Chapter 1

Introduction

1.1 Superparamagnetism

The term superparamagnetism [1] is associated to a phenomenon typical at the nanoscale and attributed to the peculiar behavior exhibited by nanometer sized grains of magnetic materials such as cobalt, nickel, iron and some alloys and oxides, among others. It is known that a particle of magnetic material, below a critical particle size, D_{C}, the normal microscopic multidomain ferromagnetic (FM) structure is energetically unfavorable and thus it contains only a single magnetic domain. This means that such a particle will posses a uniform magnetization. This critical particle size can be calculated easily accounting for the intrinsic properties of the material such its saturation magnetization, their crystalline anisotropy or the exchange stiffness contributions [2]. As particle size decreases within the single domain range, another critical threshold is reached, D_{SP}, at which the remanence and coercitivity go to zero and the particle falls into the superparamagnetic (SP) state. A sketch illustrating this transition is provided in Fig. 1.1. In this situation, for a sufficiently small magnetic particle, the energy required to reverse its magnetization is smaller than the thermal energy. Then, the magnetic dipole randomly rotates changing its orientation.

From a phenomenological point of view, one can see superparamagnetism as a reversible magnetization process. Under the effects of an external magnetic field, the induced magnetic moment of a superparamagnetic particle follows the magnetic field direction. Once this magnetic field is removed, the magnetization of this particle will fall to zero (no remanence), independently of the strength of the applied field. This lack of magnetic memory was initially perceived as an inconvenient feature (for instance, it limits the size of a physical bit in a real device). However, this superparamagnetic behavior has also some advantages over traditional ferromagnetism. For instance, the absence of remanence and coercitivity facilitates the fine tuning of the magnetization of the particle by external magnetic fields and the magnetization values achieved in the superparamagnetic state are in the range of typical ferromagnetic materials (hence the term superparamagnetism).

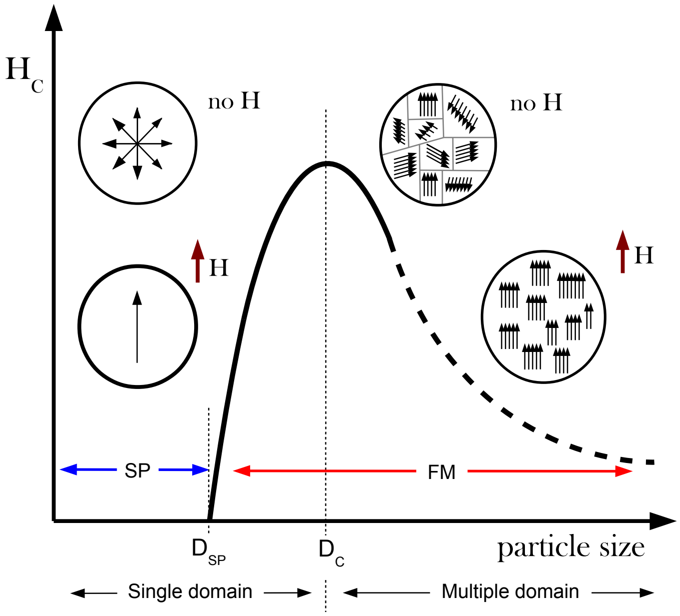

Figure 1.1: Schematic representation of the change on the coercitivity field H_C as a function of particle size. The maximum of the coercitivity field corresponds to the critical D_C size of the material, a situation in which a magnetic particle consists of a single magnetic domain. For smaller particles, the transition to the superparamagnetic state D_{SP} appears when the thermal energy suffices to flip the magnetization state, overcoming the anisotropic energy barrier, a situation corresponding to zero coercitivity field and zero magnetic remanence.

1.1.1 Relaxation mechanisms

Néel relaxation

As we have mentioned, an external magnetic field applied on a superparamagnetic particle will cause its magnetic moment to align with the magnetic field. However, after removing the magnetic field applied, thermal fluctuations causes its direction of magnetization to undergo a sort of Brownian rotation, as Néel[1] pointed out in 1949.

---

[1] Louis Eugène Félix Néel (1904 - 2000), French physicist.

Hence, after removing the applied magnetic field on an ensemble of superparamagnetic particles, a sufficient number of particles must reverse their magnetic dipole by thermal activation. To do so, the magnetic dipole must overcome the anisotropic energy barrier. For a crystal with cubic symmetry this energy barrier is KV (where K is the *anisotropy constant* and V its volume) with a probability for the process proportional to $\exp(-KV\ \ k_BT)$ where $k_B \approx 1\ 38 \times 10^{-23}$ JK^{-1} is the Boltzmann constant. In this way, one should understand this reorientation of the magnetic moment as a relaxation mechanism which depends on the particle volume (hence the existence of a critical particle size for the superparamagnetic transition, sketched in Fig. 1.1) and on the temperature.

Lets consider an assembly of aligned uniaxial particles that are fully magnetized along their easy symmetry axis. After removing the magnetic field applied, the resulting remanence magnetization M_r will vanish as a result of a relaxation process and can be described as:

$$M_r(t) = M_{sat}e^{-t/\tau_N} \tag{1.1}$$

where M_{sat} is the magnetization of the sample at saturation and τ_N is the relaxation time for the process given by:

$$\tau_N = \tau_0 e^{KV/k_BT} \tag{1.2}$$

where τ_0 is a frequency factor of the order of 10^{-9} s. This exponential dependence of τ_N on particle's volume and temperature implies that superparamagnetism is a phenomenon which also depends on the measuring time. Let us imagine that the magnetization of a single superparamagnetic nanoparticle is measured and let us define τ_m as the measurement time. If $\tau_m \gg \tau_N$, the nanoparticle magnetization will flip several times during the measurement and then, the measured magnetization will average to zero. If $\tau_m \ll \tau_N$, the magnetization will not flip during the measurement, so the measured magnetization will be what the instantaneous magnetization was at the beginning of the measurement. In the former case, the nanoparticle will appear to be in the superparamagnetic state whereas in the latter case it will appear to be *blocked* in its initial state. A transition between superparamagnetic and blocked state occurs when $\tau_m = \tau_N$. Then, a typical characterization of the superparamagnetic behavior of a material can be adopted by defining its corresponding *critical particle size* D_{SP} as the maximum particle size for which the ferromagnetic to superparamagnetic transition is observed at room temperature (typically assuming a measurement time $\tau_m \sim 100$ s [3]). Alternatively, since this transition is thermally activated, one can also adopt a different characterization by keeping this measurement time constant while varying the temperature. Thus, the transition between the superparamagnetism to the blocked state can be seen as a function of the temperature and particle size. The temperature for which $\tau_m = \tau_N$ is called the *blocking temperature* T_B, and it is given by:

$$T_B = \frac{KV}{k_B \ln(\tau_m\ \ \tau_0)} \tag{1.3}$$

From Eq. 1.3 one should notice that this blocking temperature is proportional to the volume of the sample. Then, since the superparamagnetic transition occurs for very small particles, one expects very low blocking temperatures for such systems. Thus, one has to keep in mind that since the relaxation time τ_N depends exponentially on the energy barrier KV (and hence, on the volume of the particle) narrow size distributions are required to reproducibly control the magnetic behavior of superparamagnetic particles.Typically, the characterization of a superparamagnetic sample is done by measuring the magnetization curve at different temperatures and by measuring the blocking temperature. A typical example of the measurement of a real superparamagnetic sample is shown in Fig. 1.2.

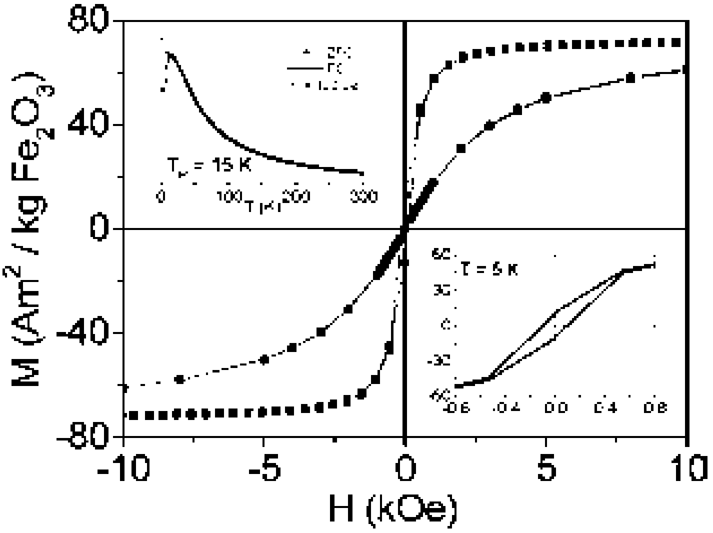

Figure 1.2: Magnetization loop obtained with a *Superconducting Quantum Interference Device* (SQUID) magnetometer at $T = 298\text{K}$ (circles) and $T = 5\text{K}$ (squares) for Fe_2O_3 nanoparticles of 5nm in size. The upper inset shows the *Zero-Field Cooling, Field Cooling* (ZFC-FC) curves used to determine the blocking temperature T_B of the sample. The lower inset shows a closer view of the magnetization curve at $T = 5\text{K}$, where a certain remanence is observed (figure extracted from [4]).

Brownian relaxation

In many situations one is interested in superparamagnetic nanoparticles immersed in a carrier liquid, what is usually known as *magnetic colloidal dispersion.* In this case, an additional relaxation mechanism for the magnetization arises due to the possible rotation of the particles inside the fluid. This relaxation mechanism, usually named *Brownian relaxation*, consists of the physical rotation of the individual particles respect to the surrounding fluid, while the magnetic moment remains blocked respect to the particle structure after removal of the magnetic field. This mechanical relaxation process can be treated in the way Debye[2] treated the dielectric properties of solutions containing molecules with permanent electric dipole moments. In this case, it is the viscosity η of the medium that opposes to the rotation of the magnetic particles and the relaxation time can be estimated as:

$$\tau_B = \frac{4\pi R_H^3 \eta}{k_B T} \tag{1.4}$$

where R_H is the *hydrodynamic radius* of the magnetic nanoparticle (the effective radius of the particle, accounting also for the increase due to the possible adsorption of solvent molecules at the particle's surface). Brownian relaxation is typically slower than the Néel relaxation mechanism and these differences between both mechanism are the basis of some relaxometry experiments of superparamagnetic nanoparticles suspensions [5, 6].

1.1.2 Magnetization at thermal equilibrium

The magnetic behavior exhibited by superparamagnetic nanoparticles is typically described following an approach similar to the one presented in 1905 by Langevin[3] to account for the description of atomic paramagnetism. Lets start by considering a superparamagnetic particle with total magnetic moment μ directed at an angle θ respect to an applied field H. If there are no additional anisotropic terms, the magnetic energy of this particle is given by $-\mu H \cos\theta$. An assembly of such particles at temperature T in thermodynamic equilibrium, will be described by a Boltzmann distribution of θ's over the particle ensemble. Averaging the $\cos\theta$ over the Boltzmann distribution gives us the fraction of the total magnetization that has been aligned by the field. The dependence of the magnetization of the ensemble on the magnetic field applied is described by:

$$M(H) = M_{sat}\mathcal{L}\left(\frac{\mu H}{k_B T}\right) \tag{1.5}$$

where $\mathcal{L}(x)$ is the familiar Langevin function defined as:

$$\mathcal{L}(x) = \coth x - \frac{1}{x} \tag{1.6}$$

For low fields, this function can be approximated to $\mu H \;\; 3k_BT$ (linear regime), and for high fields it gives $1 - k_BT \;\; \mu H$ (saturation regime). In Fig. 1.3 we show an example of a typical magnetization behavior of a superparamagnetic sample obtained from SQUID measurements at ICMAB. In this case, the Langevin function defined in Eq. 1.6 accurately describes the magnetization as a function of the magnetic field applied. This treatment is analogous to the Langevin treatment of paramagnetism, although different in nature. It differs in the sense that the moment μ we are dealing with is not that of a single atom, but rather of a single domain ferromagnetic particle, which may contain more than 10^5 atoms ferromagnetically coupled by exchange forces.

---

[2] Petrus Josephus Wilhelmus Debye (1884 - 1966), Dutch physicist and physical chemist.

[3] Paul Langevin (1872-1946), French physicist.

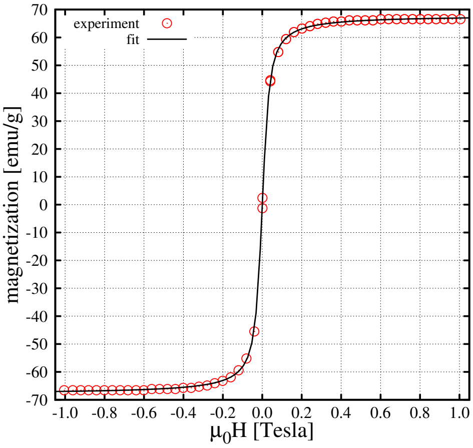

Figure 1.3: Magnetization curve for the 12 nm γ-Fe_2O_3 nanocrystals presented in the supplementary material of Ref. [7]. Symbols are experimental data obtained from SQUID magnetometer measurements at 298K and the solid line is the corresponding fit to a Langevin function according to Eqs. 1.5 and 1.6.

However, in some situations, this rather simple description does not suffice to account for the complete characterization of the magnetic response of the superparamagnetic particles. It has been experimentally observed that some discrepancy can arise as a consequence of different factors: the presence of demagnetization effects due to changes on the crystalline structure of the particle's surface (and hence on the magnetic properties) and/or a distribution of particle's sizes in the sample (and hence a distribution of particle moments). In these situations, more accurate models can be used to account for different effects, such as different distributions of particle size or the inner structure in composite nanoparticles [8]. In some cases, one can even take advantage of these discrepancies, since they yield information about the width of the size distribution [8, 9]. It is known that various parts of the magnetization curve can be used to obtain various averages over the particle size distribution. The initial susceptibility is sensitive to the larger particles present in the sample, whereas the approach to saturation is largely governed by the smaller particles.

Summarizing, and as an operational definition of superparamagnetism, a superparamagnetic particle has to fulfill at least two requirements. First, the magnetization curve must show no hysteresis since that is not a thermal equilibrium property, i.e., at zero field the macroscopic magnetization must be zero. In the presence of an external magnetic field, large saturation values of the magnetization must be obtained (orders of magnitude larger than those typical of paramagnetic materials). Second (and assuming non-interacting particles) the magnetization curve for an isotropic sample must be temperature dependent to the extent that curves taken at different temperatures must approximately superimpose when plotted against H T [1].

1.1.3 Superparamagnetic nanoparticles

One of the first and most easily prepared magnetic colloidal system was developed by Steven Papell of the National Aeronautics and Space Administration in the early 1960's. Papell's colloid consisted of finely divided particles of magnetite (a molecular mixture of iron oxides FeO and Fe_2O_3) suspended in kerosene. To keep the particles from clumping together or settling out of suspension Papell added oleic acid, an organic substance that served as a surfactant or dispersing agent. Similar magnetic dispersions were also synthesized with different nanometer sized particles of pure compounds, like iron, nickel or cobalt [10] in a wide range of carrier liquids [11].

Nevertheless, in most applications, superparamagnetic colloidal dispersions with large magnetic response are required. Since the magnetization of a particle is proportional to its volume, the maximum magnetization that one can achieve is limited by the critical size of the superparamagnetic transition, which is different for different materials [3]. A well stablished strategy to create superparamagnetic particles with larger superparamagnetic response are what are called *composite nanoparticles* (see Fig. 1.4). These superparamagnetic composites are typically made by embedding superparamagnetic nanocrystals in a non-magnetic matrix, such as polystyrene, nanoporous silica or others) [2, 4, 12–14]). The resulting colloidal particles retain the superparamagnetic response of their constituent nanocrystals and show a very large magnetization in presence of external magnetic fields but no coercitivity nor remanence at the working temperature. However, in these situations, the typical Langevin description provided (Eqs. 1.5 and 1.6) does not always suffice to accurately represent the magnetization curve for such particles. Apart from the intrinsic superparamagnetic behavior of the constituent nanoparticles, one has to account for other particle-particle interactions (for instance, interactions between the nanoparticles inside the skeleton matrix due to their proximity) or surface effects due to the coating, which can lead to changes in the overall magnetic response of the colloidal particle.

Here we would like to note that, due to the different design of magnetic colloidal particles and their corresponding applications, the number of different names for a magnetic colloid is also large and could be confusing. In general, and in order to clarify the terminology adopted in this work, we will reserve the term *composite* for a structured superparamagnetic particle, either being core-shell or matrix-dye synthesized. We will use the term *nanocrystal* for single domain superparamagnetic particles or stable clusters of them, with no specific shell or matrix (i.e. only stabilization agents). Depending on the application context, other names can be found in literature applied either to nanocrystals or composites. For instance, in the biotechnological field is often used the term *magnetic bead* or *magnetic carrier* to refer to magnetic colloidal entities dispersed in a fluid medium. In situations in which the individual colloidal particles have no relevance by themselves, but rather together with the carrier fluid, the term *ferrofluid* is generally adopted.

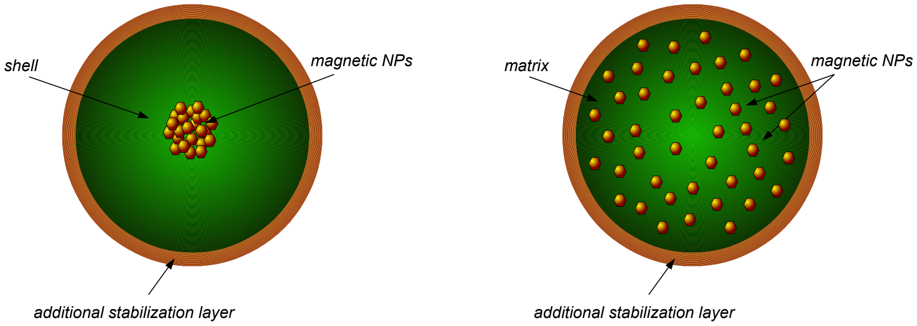
shell
magnetic NPs
additional stabilization layer
matrix
magnetic NPs
additional stabilization layer

Figure 1.4: Different strategies can be adopted in the design of composite superparamagnetic colloidal particles. A first approach namely *core-shell* is the coating of a magnetic core formed by some superparamagnetic particles with some non-magnetic layer. A second approach namely *matrix-dye* consists of embedding superparamagnetic nanoparticles in a non-magnetic porous matrix.

1.1.4 Applications

Magnetic nanoparticles are emerging key ingredients in the development of new functional materials designed for specific applications [15]. This is reflected in the large number of companies (Chemicell, BASF, Invitrogen, Estapor, MagnaMedics, among others) that distribute commercial nanoparticles designed to target specific applications in a vast variety of fields [16]. The improvement and discovery of new nanoparticle's synthesis methods has lead to a major control over the particle properties, morphology and sample polydispersivity [17]. These progresses boosted the development of new applications taking advantage of these new materials. In table 1.1 we show a summary of some examples of different superparamagnetic particles, with different morphology, coatings and magnetic properties, designed to target specific applications and fulfilling the corresponding requirements, such as biocompatibility, high colloidal stability or monodispersity. Some specific applications are commented next.

For instance, magnetic ferrofluids have been presented as novel functional materials in the optical field. Their magneto-optical properties are determined by the nature, contents and structuration of the magnetic particles in the carrier liquid. During the early 80's the study of magnetically induced birefringence, dichroism, Faraday rotation and other magneto-optical effects in magnetic fluids was relatively new. Experimental evidences pushed the attention of researchers on the development of new magneto-optical devices based on magnetic fluids technology [28]. Mostly, the new applications are based on the tunability of the refractive index of the ferrofluid due to the chaining structures

Table 1.1: Examples of different superparamagnetic particles designed to target specific applications, covering a wide range of sizes, coatings and magnetic saturation values. Typically, the character @ is used to differentiate the core (or dye) composition and the shell (or matrix) nature.

composition	size [nm]	M_{sat} [emu/g]	morphology	application	ref.
γ-Fe_2O_3	12	68.0	nanocrystals	separation	[7]
γ-Fe_2O_3	15-20	50.0	nanocrystals	MRI	[18]
γ-Fe_2O_3@Polymer	134	12.7	matrix/dye	photonics	[19]
γ-Fe_2O_3@SiO_2	82	4.4	core/shell	MRI	[20]
γ-Fe_2O_3@SiO_2	157	3.7	core/shell	MRI	[20]
γ-Fe_2O_3@SiO_2	150	3.4	core/shell	separation	[21]
Fe_3O_4@Polymer	100	6.0	matrix/dye	separation	[22]
Fe_3O_4@Polymer	80-200	30-60	core/shell	MRI	[23]
Fe_3O_4@Carbon	25	42.2	core/shell	photonics	[24]
Fe_3O_4@Polymer	67	76.1	core/shell	tracking	[25]
Ni@SiO_2	55	50.0	core/shell	separation	[26]
CeO_2 (Fe doped)	10	6.0	nanocrystals	general	[27]

induced by the application of an external magnetic field. A large amount of magneto-optical applications are based on this effect: tunable beam splitters, optical gratings, optical-fiber modulators, magneto-optical wavelength filters, tunable interferometers and sensors [29, 30].

Another approach to magneto-optical devices is the fabrication of magnetically controllable photonic crystals, formed by self-assembly of high charged, monodisperse superparamagnetic colloidal spheres [19] also called *Crystalline Colloidal Arrays* (CCA). For instance, in the case of iron oxide particles in aqueous solution, external magnetic fields can be used to induce strong attractive forces between neighboring magnetic particles, bringing them close to each other. In order to stabilize such structures, electrostatic repulsive forces are introduced by coating the particles with a layer of polyelectrolyte containing high density negative charges. The two forces reach a balance, eventually organizing the particles into long chains with equal interparticle separations. The diffraction from these superparamagnetic CCAs can be controlled by the imposition of magnetic fields which readily alter the CCA lattice constant. It has been shown that the addition of magnetic components to the colloidal building blocks provides a wide tuning range covering the entire visible spectrum, a fast and fully reversible response, and the compatibility with miniaturization for device fabrication [31, 32].

A different strategy, mostly used in biotechnological applications, is to endow the individual colloidal particles with specific functionalities rather than a collective property emerging from the whole dispersion (see Fig. 1.5). For instance, in biomedical applications [33, 34], superparamagnetic colloids can be functionalized onto their surface by adsorption of different molecules or chemical groups, specific for each particular

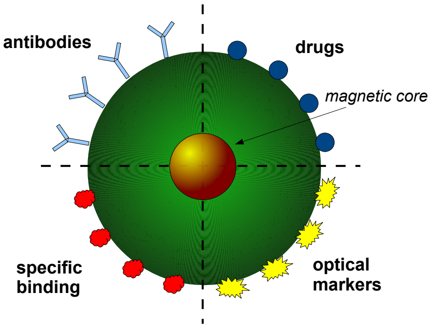

Figure 1.5: Magnetic nanoparticles are often decorated onto their surfaces with specific ligands or chemical groups (sometimes with more than one at a time) which confer specific functionalities required in different applications.

application [35]. The functionalization with appropriate biocompatible molecules (phospholipids, immunospecific agents, etc.) allows the binding to specific targets, from chemical pollutants to proteins or specific cells, opening the possibility of selective separation and purification of non-magnetic entities. In some cases, superparamagnetic colloids are also functionalized by incorporating quantum dots (QDs) onto the surface of the colloid, enabling the optical monitoring of each individual particle [36]. For instance, Yavuz and coworkers [37] reduced the mass of waste associated with arsenic removal from water by orders of magnitude by using high specific surface area superparamagnetic nanoparticles. A different example was the recovering of microalgae Chlorella sp. (used in biodiesel production) from culture media by Lim *et al.* [38]. The efficiency of the process was as high as 99% and it was accomplished by binding iron oxide nanoparticles (NPs) to microalgae cells in the presence of a polyelectrolyte as a binder. The impact of the magnetic separation technology in different fields is reflected in several reviews, covering the main aspects involved in magnetic separation, from large industrial processes to batch biotechnological applications [39, 40] or biomedicine [33, 34, 41, 42].

During last decade, superparamagnetic nanoparticles have been widely used in biology and medicine in very different applications: biomolecule purification and cell separation, as *Magnetic Resonance Imaging* (MRI) contrast agents, as biomagnetic sensors, in magnetic hyperthermia for cancer treatment and drug delivery and transfection [33]. In all these applications, the aggregation or clustering induced by the external magnetic field applied can have strong effects by altering interparticle interactions, creating clusters which are subject to size and shape dependent forces. For example, iron oxide magnetic nanoparticles have been proposed as suitable candidates for MRI contrast agents due to their high magnetic susceptibilities. The formation of aggregates induced by the magnetic field and/or the polymer coatings can be a dominant factor in determining de relaxivity 1 T_2 and needs to be considered [43, 44]. Carroll and coworkers [45], studied the effects on the relaxivity 1 T_2 of different polyether coating loadings in iron oxide nanoparticles. They found that for such particles, the primary mechanism driving variations in proton relaxivity is the level of aggregation within the systems. Any changes to the exclusion or diffusion of water molecules from variations in the polyether loadings are either minor or cancel each other, and therefore have a minor effect on the $1/\mathrm{T}_2$ relaxivity in comparison with the effects of aggregates. Hence, MRI contrast agents could be designed either to remain completely dispersed or to aggregate purposefully to maximize contrast.

A different example is which this aggregation could lead to important effects is the *Magnetic Relaxation Immunoassay* (MARIA), a detection technique based on magneto-relaxometry experiments, i.e. the measurement of the relaxation of the net magnetic moment of the magnetic nanoparticles in solution. In this technique, one measures the relaxation curves for a solution of magnetic particles (designed to bind to some specific molecule or entity) in two different situations. A pure solution of the colloidal magnetic particles and the same dispersion in which the target entity is also present. For unbound magnetic particles in solution, the dominating relaxation mechanism is via Brownian relaxation. The binding of large targets to the magnetic particles strongly decreases their Brownian relaxation, so that they relax predominantly via Néel relaxation process. By separating the two distinct relaxation curves, the amount of bound magnetic nanoparticles can be quantified [5, 6].

1.2 Magnetic Colloidal Dispersions

Since ferromagnetism is a property of iron, nickel, cobalt and some other compounds and alloys of these elements, one approach to create a magnetic fluid might therefore be to heat one of those metals until it becomes molten but, unfortunately this strategy cannot work. The reason is that the ferromagnetic behavior disappears above a certain temperature, called the Curie point, which is invariable well below the melting point of the material. It is possible nonetheless to create a stable magnetic fluid by adding magnetic particles in a liquid carrier, as it has been already mentioned. Such mixture consisting of a dispersed phase (or discontinuous phase) distributed uniformly in a finely divided state througout a dispersion medium (or continuous phase) is what is known as *colloid*[4] or *colloidal dispersion.* Some examples of colloidal dispersions are aerosols, gels or emulsions and their properties are subject of standard textbooks [46].

---

[4] Even Michael Faraday (1791-1867) was the first to discover the first metallic colloid (gold suspended in water) he did not use the term "colloid", which was coined by Thomas Graham (1805-1869) in 1861.

1.2.1 Stability

An important feature of disperse systems is the large area of the interface between the particle or droplet and the surrounding medium. Consequently, a significant proportion of the molecules are associated with the microheterogeneous regions which form the interfaces between the dispersed phase and the dispersion medium. The amount of work W needed in a process carried out isothermally is equal to the increase in free energy of the system. In a process in which a certain increase of surface area is achieved, the increase in free energy is proportional to the surface created, A, and it is called surface excess free energy, ΔG_{exc}:

$$\Delta G_{exc} = W = \sigma A \tag{1.7}$$

where the proportionality factor σ is called the *surface* or *interfacial tension*. Thus, the increase in free energy arises from the difference between the intermolecular forces experienced by surface molecules compared with those acting on them when they are part of the bulk material. It is then clear that a colloidal dispersion represents a state of higher free energy than the corresponding to the material in bulk. Passage to a state of lower free energy will therefore tend to occur spontaneously, where particles aggregate in order to minimize the surface A. This process is known as *flocculation*. Typically, an energy barrier is imposed to avoid this aggregation, preventing the elimination of such colloidal state. In presence of such a barrier the system will be metastable and may remain in that state for a long time (this stabilization mechanism is usually known as *kinetic stabilization*).

There are two general strategies to stabilize a colloidal dispersion and avoid its flocculation, namely *electrostatic stabilization* and *steric stabilization*. Electrostatic stabilization is based on the repulsive force arising between electrical charges with equal sign. In general, the stability of the particles is achieved by covering the particle's surface with ions or charged groups (either positively or negatively charged), conferring a net surface charge to the particle and creating a repulsive force between them, able to overcome the van der Waal forces. Differently, steric stabilization consists of covering the particles with sufficiently large molecules (typically polymers) preventing the particles to get close in the range of attractive forces. In Fig. 1.6 we show a scheme of the potential energy landscapes corresponding to both stabilization strategies. Despite both strategies effectively stabilize the colloidal dispersion, some important differences arise due to their different nature. The most important difference between them is that the steric stabilization presents a virtual infinite energetic barrier while a finite energy barrier appears in the electrostatic case. Then, the integrity of a steric-stabilized colloid depends directly on the integrity of the stabilization layer. Differently, the energy barrier in the electrostatic case can be modified by the addition of salts or changing the pH of the solution to effectively neutralize or *screen* the surface charge of the particles. A reduction on this energy barrier could diminish the repulsive forces that keep colloidal particles separated and allow for flocculation due to van der Waals forces. This flocculation phenomenon has to be understood as an irreversible aggregation

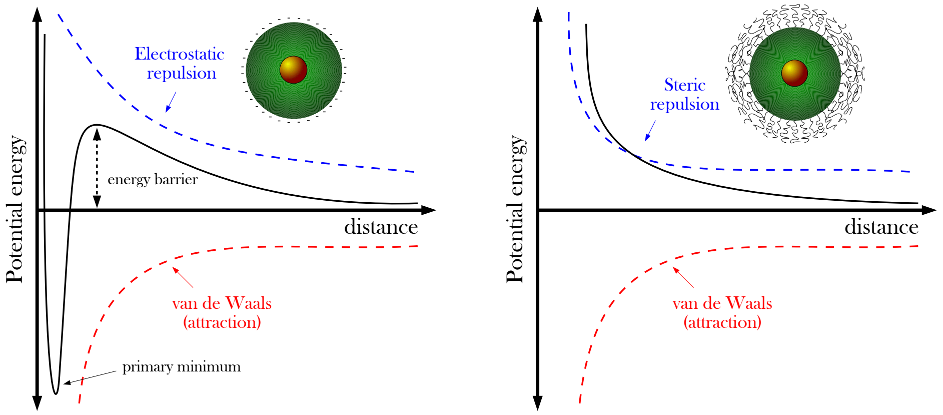

Figure 1.6: Schematic plot of the typical potential energy landscape close to the surface of a colloidal particle stabilized through two different strategies: *electrostatic stabilization* (**left**) and *steric stabilization* (**right**). In the first approach, the surface of the particles are coated with charged molecules or groups, conferring a net surface charge to the particles. In this situation, the energy barrier can be adjusted by varying the properties of the solvent. A second strategy is to cover the surface of the particle with large molecules, avoiding the particles to get close enough and overcome the van der Waals attraction at short distances.

process, since particles get trapped into the primary minimum. After flocculation, the initial dispersion can be typically recovered by methods such as sonication.

Secondary minimum

Dispersions of superparamagnetic colloids require the application of an external magnetic field in order to induce structuration (aggregation or chain formation) as the colloids have no magnetic dipole in the absence of external field. This contrasts with ferromagnetic colloids, which exhibit aggregated structures in the absence of an external magnetic field as a consequence of their permanent magnetic dipole. In absence of an applied magnetic field, superparamagnetic nanoparticles have no net magnetic dipole so that the magnetic force among them is zero. Then, a well stabilized superparamagnetic colloidal dispersion is homogeneous with no clustering of particles. When a magnetic field is present, superparamagnetic colloids acquire an induced magnetization pointing along the applied magnetic field, and then aggregation is possible. In general, the force between two dipolar particles is represented by the anisotropic magnetic dipole-dipole interaction, which depends on the orientation of the dipole moments of each particle and their relative distance (see Fig.1.7). The corresponding magnetic energy between two interacting dipolar particles is:

$$U_{dd} = \frac{\mu_0}{4\pi}\frac{1}{r_{ij}^3}\left[(m_i \cdot m_j) - 3(m_i \cdot \hat{r}_{ij})(m_j \cdot \hat{r}_{ij})\right] \tag{1.8}$$

where m_i and m_j are the magnetic moments of particles i and j, respectively, and r_{ij} is the vector distance between their centers. In the case of two identical superparamagnetic particles (equal radius and magnetic moment $m = m_i = m_j$) under the effects of an external magnetic field, this last equation reduces to:

$$U_{dd} = \frac{\mu_0}{4\pi}\frac{m^2}{r_{ij}^3}[1 - 3\cos^2\theta] \tag{1.9}$$

where θ is the angle between the direction of the external magnetic field applied and the line joining the centers of both dipolar particles (Fig. 1.7 a). Clearly, the minimum energy configuration corresponds to $\theta = 0$ and an interparticle distance of $2a$ (where a is the radius of the particles). Therefore, two interacting particles in solution under a sufficiently high magnetic field will tend to aggregate *head-to-tail* in order to minimize the magnetic energy, forming chain-like structures (Fig. 1.7 b). For large magnetic fields, these structures become more stable and the former particles align leading to most robust and straight chains (Fig. 1.7 c).

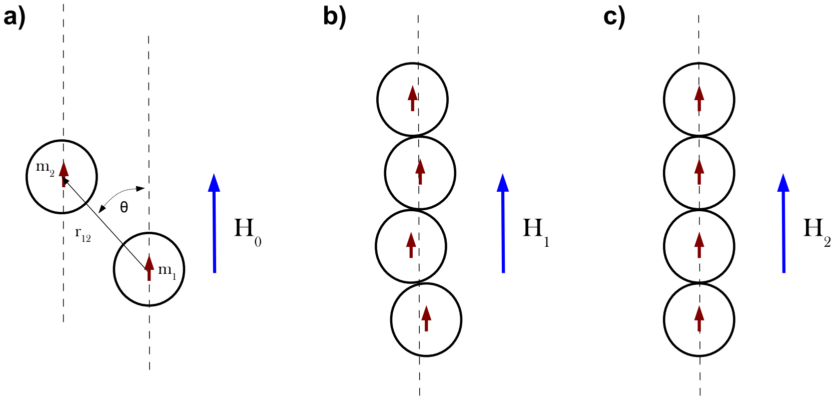

Figure 1.7: Scheme representing the interaction between superparamagnetic particles in different situations with $H_0 < H_1 < H_2$. **a)** Under the effects of an applied magnetic field (H_0), dipolar particles will tend to align along the magnetic field direction with an interaction magnetic energy given by Eq. 1.9. **b)** If the magnetic field is strong enough (H_1), these magnetic particles will align head-to-tail, forming chain-like structures. **c)** The structures formed will become more stable for higher magnetic fields (H_2).

Therefore, when an external field is applied, the dipolar interaction between superparamagnetic particles generates a secondary minimum in the energy landscape (see Fig. 1.8) which enables the particles to bind each other forming chains or other structures. However, the magnetic interaction must be large enough so as to overcome thermal agitation, which tends to destroy them. One defines the strength of the interparticle interaction by comparing the minimum in the magnetic energy between two identical particles in contact (in absolute value) with the thermal energy. This definition has been extensively used in different studies of ferromagnetic and superparamagnetic colloidal suspensions [47–50]. Given two identical particles with magnetic susceptibility $^{\rightarrow}$ and radius a, and assuming that the magnetization of the particles follows a linear dependence on the magnetic field applied, H (i.e. valid for low fields), the magnetic strength is defined as:

$$\lambda = \frac{\pi \mu_0 a^3 {}^{\rightarrow 2} H^2}{9 k_B T} \tag{1.10}$$

where μ_0 is the *permeability* of the free space. In general, the typical magnetic field required to bring a superparamagnetic particle to saturation is roughly about 0.1 T, i.e. the linear magnetization regime (characterized with the magnetic susceptibility of the particle) ends up around this value and an increment on the external magnetic field applied will not produce a higher magnetization. Thus, and analogously to Eq. 1.10, we proposed the following expression to define the magnetic strength parameter, valid for larger values of the magnetic field applied (i.e. in the saturation regime):

$$\Gamma = \frac{\mu_0 m_s^2}{2\pi (2a)^3 k_B T} \tag{1.11}$$

where m_s is the magnetic moment at saturation. Physically, $\Gamma \gg 1$ corresponds to a situation in which the magnetic interactions dominate the behavior of the system, while for $\Gamma \ll 1$ thermal agitation dominates the motion of the particles in solution and one does not expect aggregation.

In case of chain formation, it is important to notice that the chaining process is reversible. In effect, if these magnetic forces are removed by eliminating the external field, the initial energy barrier is recovered (the secondary minimum vanished) and the chains disaggregate, recovering the initial colloidal dispersion. In Fig. 1.8 we show the calculation of the potential energy for a superparamagnetic colloid of 100 nm size. In it, we have taken into account the attractive and repulsive contributions according to the DLVO (*Derjaguin, Landau, Verwey, Overbeek*) theory together with the magnetic contribution. Then, under sufficiently large magnetic fields, the dipolar interactions between particles suffice to drive colloidal particles to form chain-like structures [51, 52]. These chains are aligned with the external magnetic field both in the case of homogeneous [50, 53, 54] and inhomogeneous magnetic fields [52, 55, 56]. After removal of the external magnetic field, it is observed that the chains rapidly disaggregate and the initial dispersion is recovered.

Martinez-Pedrero *et al.* [53, 57–59] showed by experiments that the aggregation phenomenon can move from reversible to irreversible by changing the electrolyte concentration in superparamagnetic dispersions. The aggregation process was monitored by *Dynamic Light Scattering* (DLS) and the effective diffusion coefficients were assessed as

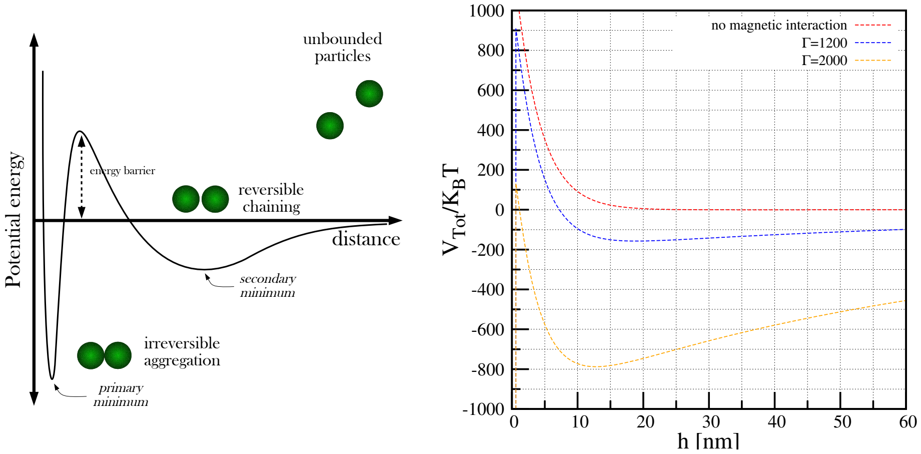

Figure 1.8: Left: Scheme showing a secondary minimum in the energy landscape of a magnetic particle due to the magnetic anisotropic energy contribution. The reversible chaining process between superparamagnetic colloids under the effects of an external magnetic field is related to the existence of this secondary minimum. **Right:** Interaction potential at short distances between two superparamagnetic particles of radius 100 nm and different values for the magnetic strength. The potential energy is calculated as the sum of the attractive van der Waals interactions, the repulsive electrostatic interactions according to the DLVO theory and the potential magnetic energy between particles (Eq. 1.9). The figure on the right is a modification of figure 3 from Ref. [51].

a function of time. Adding electrolytes at different concentrations [58] they controlled the electrostatic interaction between particles and showed that it can induce irreversible bonding [60]. They observed for electrolyte concentrations lower than 0.50 mM, that the initial dispersion is recovered after removal of the magnetic field. However, at larger electrolyte concentrations, the chains break up only partially, remaining a certain amount of chains in solution. For even higher electrolyte concentrations (50 mM), no breack up of the chains was observed after the magnetic field was turned off, thus showing a completely irreversible aggregation. The overall stability of the different linear structures was studied in the framework of the DLVO theory.

1.2.2 Structure formation under magnetic fields

The structuration phenomena in magnetic colloidal suspensions have been the interest of research groups for scientific and technological reasons during the last 40 years. In a seminal article by De Gennes and Pincus [47], it is conjectured that a colloid formed of identical spherical ferromagnetic particles suspended in a magnetically passivated liquid tends to form chains along the direction of the magnetic field. In their pioneer work, they focused the attention on the equation of state for two limiting cases. They argued that under high external magnetic fields and low concentrations, the ferromagnetic grains tend to form chains along the direction of the magnetic field. At zero field, some chains are still present but oriented with no preferred orientations and in competition with closed ring and cluster structures. This model was discussed in detail for the low temperature region, in which the dipole-dipole interactions between grains are large, and the possibility of a liquid-like phase was suggested due to the similarity of this interaction to a van der Waals attraction [47]. They provided the following expression to evaluate the mean chain length N expected in equilibrium:

$$N = \left[1 - \frac{2\pi_0}{3\lambda^2} e^{2\lambda} \right]^{-1} \tag{1.12}$$

where λ is the magnetic strength parameter defined in Eq. 1.10 and π_0 is the initial volume fraction of colloids defined as the volume occupied by the total number of particles n with diameter d in the system respect to the total volume:

$$\pi_0 = \frac{nV_p}{V_{tot}} = \frac{n\pi d^3}{6V_{tot}} \tag{1.13}$$

Notice that in Eq. 1.12, a divergence appears depending on the values for the volume fraction of particles (π_0) and the magnetic strength (λ). They interpreted the divergence in Eq. 1.12 as the onset of a gas-liquid phase transition.

This pioneer work of De Gennes and Pincus [47] was the basis for a series of different experimental and theoretical works which focused their attention on the association phenomenon in magnetic fluids [48, 61]. For instance, Fermigier and Gast [62] conducted different experiments describing optical microscope observations of the structures

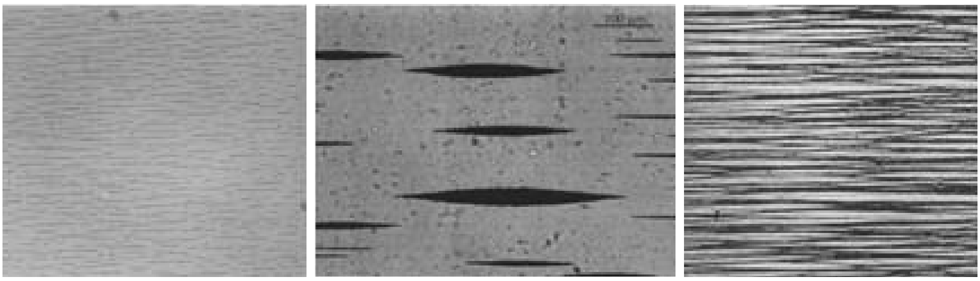

Figure 1.9: Different real structures found in suspensions of superparamagnetic particles. **Left:** Chains formed in a suspension of $\phi_0 = 0.023$ and field strengh $\lambda = 19.5$ [62]. **Center:** Bundles obtained for a suspension with volume fraction $\phi_0 = 0.005$ and field strength $\lambda = 37$, with an pulsed magnetic field at frequency $\nu = 2$Hz [63]. **Right:** Fibrous structure under a field strength of $\lambda = 285$ and high concetration ($\phi_0 = 0.69$) [62].

formed by superparamagnetic polystyrene particles suspensions loaded with iron oxide grains (see Fig. 1.9). They analyzed the expected phase transition at low field strength for their superparamagnetic dispersions. They found that, for large fields (when the dipolar strength greatly exceeds thermal energy i.e. $\lambda \gg 1$), the aggregation proceeds as a non-equilibrium transport-limited process, and the dipolar particles start forming chains aligned parallel to the magnetic field due to the dipolar interactions. For larger volume fractions they observed that these initial chains experience a sideways coalescence through a zippering motion, thickening the chains and forming *bundles*. For higher volume fractions they observed a crosslinking of the structures (chains and bundles) forming a fibrous structure. A summary of these different structures found in superparamagnetic dispersions is sketched in Fig. 1.10 as a function of volume fraction and the magnetic strength parameter. Furthermore, the time evolution of some of those structures suggested the existence of an equilibrium state, but the corresponding values for the volume fraction π_0 and magnetic strength λ were not in fully agreement with the expression proposed by De Gennes (Eq. 1.12).

Those works have motivated further studies of the aggregation structures obtained in superparamagnetic dispersions. More recently, other studies have also presented evidences of such structures in superparamagnetic dispersions. For instance, Martínez-Pedrero *et al.* studied dispersions of superparamagnetic polystyrene particles under magnetic fields at low volume fractions. They showed by *Static Light Scattering* (SLS) and *Transmission Electron Microscopy* (TEM) micrographs that the formed aggregates are chain-like shaped structures [57]. Furthermore, they also showed by DLS experiments how the length and the stability of these chains can be controlled by the addition of different amounts of electrolyte [58].

Up to this point, we have discussed the different structures that one can obtain when an homogeneous magnetic field is applied to a monodisperse superparamagnetic dispersion (i.e. same size and magnetic response). Nevertheless, a more complex

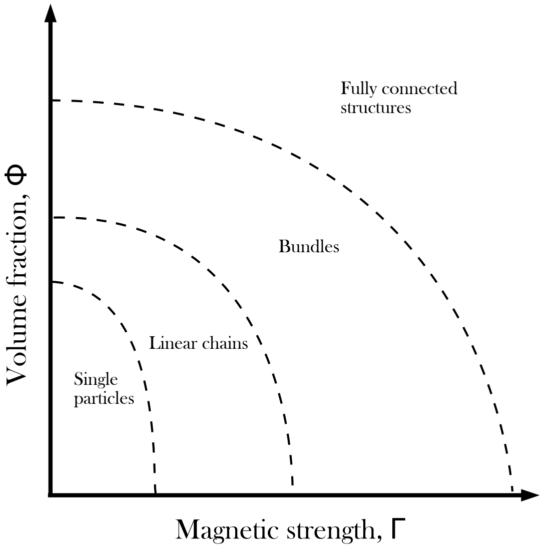

Figure 1.10: Sketch representing different structures observed in the suspension as a function of dipolar interaction parameter Γ and volume fraction, according to the suggested scheme in Ref. [62].

scenario arises in mixtures of particles with large differences in size and magnetic response. For instance, Erb and co-workers [64] showed experimentally the formation of different structures with multipole symmetry formed by mixtures of magnetic and non-magnetic particles in a ferrofluid (see Fig. 1.11). The self-assembly of such complex equilibrium superstructures is driven by the different magnetic response of the particles present in the mixture and the mismatch between their magnetic response and that from the ferrofluid. We remark here that, due to the different length scale between the size of the colloids and that from the superparamagnetic particles, the magnetic response of the fluid surrounding a colloidal particle can be approximated as the sum of contributions from each superparamagnetic nanoparticle contained in a certain volume (*continuum approximation*). Thus, the effective magnetic moment m_{eff} of a colloidal particle immersed in a ferrofluid made of superparamagnetic nanoparticles with magnetic moment m_f can be estimated as [65]:

$$m_{eff} = m_c - \frac{4}{3}\pi R_c^3 n_f m_f \tag{1.14}$$

where m_c is the magnetic moment of the colloidal particle, R_c is its radius and n_f is the number of nanoparticles (forming the ferrofluid) displaced by the colloidal particle when immersed. Notice here that this expression resembles the one corresponding to the buoyancy effect due to the mismatch in densities according to Archimedes's principle. Accompanying their experiments, they also demonstrate how the different structures

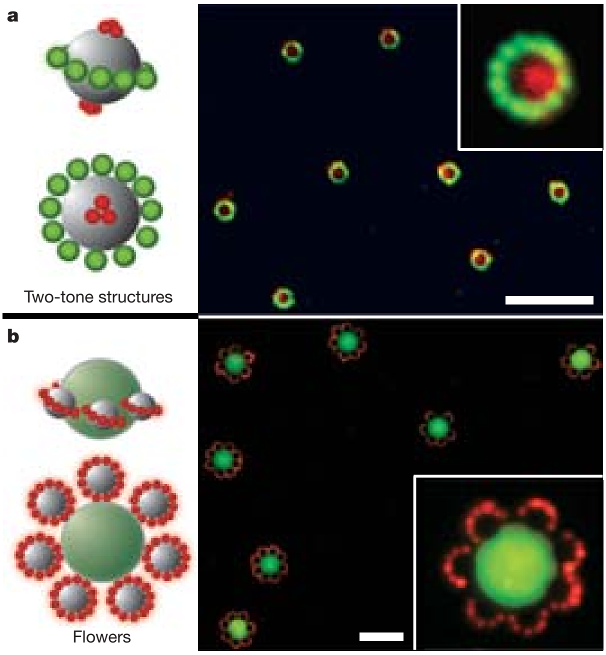

Figure 1.11: Example of complex structures obtained in mixtures of particles with different size and magnetic response induced by homogeneous magnetic fields. The fluorescent images show the structure formation in four-component colloidal-particle aqueous suspensions consisting of **a)** ferrofluids, non-magnetic particles (red 0.21 mm and green 1.0 mm) and paramagnetic core particles 2.7 mm. **b)** ferrofluid, 1.0 mm non-magnetic particles (red), 2.7 mm paramagnetic core particles and 9.9 mm non-magnetic particles (green). Each panel includes a sketch of the assembled structure and a magnified view of one of the assembled structures (inset). Scale bars, 20 mm. Figure extracted from Ref. [64].

obtained can be fine-tuned by adjusting the ferrofluid concentration [66]. The model presented, based in the continuum approximation of the local fluid magnetization was already applied to other similar situations [67–69].

These complex structures induced indirectly and formed by non-magnetic particles have also been shown to be a promising tool in tissue engineering [70]. For instance, Krebs *et al.* succeeded in the creation of ordered cellular structures with a novel strategy using inert and cyto-compatible magnetic nanoparticles. The advantage of the new approach presented was that the cellular assembly was dictated by magnetic nanoparticles, without relaying on cell binding or nanoparticles uptake. They demonstrated that the linear cell structures obtained were stable and could be further cultured without the magnetic field or nanoparticles.

1.2.3 Aggregation kinetics

As we have seen in previous section, the application of external magnetic fields induce a diversity of colloidal structures in superparamagnetic dispersions. Promislow and Gast studied the time evolution of chain-like structures in superparamagnetic dispersions under constant magnetic fields by optical microscopy experiments [50]. Specifically, they focused the attention on the kinetic growth of such structures arising for different values of the magnetic strength (defined in Eq. 1.10) and the volume fraction. To quantitatively characterize the growth of these chains, they evaluated the *average chain length* (i.e. the average number of particles in a chain) defined as[5]:

$$N \;\; = \frac{{}_s \, s n_s(t)}{{}_s \, n_s(t)} \tag{1.15}$$

where $n_s(t)$ is the number of chains of size s at a given time. They provided the first comparison of three-dimensional experimental results with computer simulations and theory. According to the their findings, they proposed that the chain growth follows a power-law behavior of the form:

$$N \;\; \sim t^z \tag{1.16}$$

where the scaling exponent z obtained in their experiments was in the range $z = 0\ 48 - 0\ 75$. They found an inverse dependence of z on both magnetic strength λ and particle volume fraction π, which they attributed to the hindered lateral diffusion of chains at high concentrations and strong magnetic fields. Nevertheless, the scaling law broke down above some critical volume fraction, and no current theory could explain this transition.

More recently, Dominguez-Garcia *et al.* [71] also performed 2D video microscopy and image analysis experiments of superparamagnetic micrometer size particles under the effects of an external magnetic field. They reported other quantities of interest which also follow a similar power-law behavior, such as the number of unbounded colloids n_1 or the *mean* (weight average) *cluster size* S defined as:

$$S \;\; = \frac{{}_s \, s^2 n_s(t)}{{}_s \, s n_s(t)} \tag{1.17}$$

They compared the experimental results with 2D Brownian Dynamics simulations with a hard sphere dipolar model, for large magnetic strength $\lambda = 48 - 3000$ and relatively high surface fractions. In view of the variety of different values for these exponents and the discrepancies between experiments and the simulations presented, they concluded that different mechanism should drive the aggregation dynamics in such systems.

Similar experimental analysis or complementary techniques have been improved for a better understanding of the aggregation mechanisms [54]. Techniques like DLS has been a useful tool to characterize time evolution of such chain-like structures [53] and the effects of the electrolyte concentrations or sedimentation in the aggregation mechanism [53,59]. For instance, DLS results from Rablau *et al.* [72] point towards a two step process, in which a fast chaining process is followed by a slower coalescence of the chains forming bundles. Similar results were also reported in Ref. [73] in which a two step process is observed in superparamagnetic dispersions of iron oxide colloids, combining *Nuclear Magnetic Resonance* (NMR) experiments and Molecular Dynamics simulations. Other experimental techniques based on *Magnetic Circular Dichroism* (MCD) have been envisaged as a fast magneto-optical characterization of superparamagnetic dispersions, opening new opportunities to characterize these aggregation mechanisms [74].

---

[5] Here we have adopted this notation in accordance with our works, and we have used the notation $\langle S(t) \rangle$ for the weight average chain size.

1.3 Magnetophoresis

As a rather simple definition, the magnetophoresis can be understood as the controlled motion of magnetic particles dispersed in a fluid medium by the application of inhomogeneous magnetic fields. The basic idea behind any magnetophoretic process is to take advantage of the different magnetic response of the colloids and the surrounding fluid under the effects of an applied magnetic field. It is known that the net magnetic force acting on a magnetic colloidal particle is a function of the difference of the particle's magnetization and the magnetization of the surrounding fluid (the origin of Eq. 1.14). Thus, the magnetic force exerted on a colloidal particle (when the variation of the applied magnetic field over the particle volume can be ignored) is typically calculated as [40]:

$$F_m = \mu_0 \left[(m_p - m_f) \cdot \quad \right] H \tag{1.18}$$

where μ_0 is the permeability of the free space, H is the applied magnetic field at the location of the particle and m_p and m_f are, respectively, the magnetic dipole moment of the colloidal particle and the effective magnetic moment corresponding to the fluid volume displaced by the colloidal particle. Two interesting observations can be made on the basis of this last expression. First, the magnetic force is proportional to the magnetic field gradient, a situation different from electrophoresis, where the force is proportional to the electric field. In magnetophoresis, the magnetic field is only responsible of the induced magnetization, and no force on the particle is produced unless a magnetic gradient is present. In the steady state, the magnetophoretic force, F_{mag}, acting on a colloidal particle is compensated by the viscous drag force, F_{drag}, exerted by the fluid. Since the magnetic force and the viscous drag force scale differently with particle size ($F_{mag} \quad d^3$ and $F_{drag} \quad d$), larger magnetic gradients and larger particles will always provide a greater magnetic response. This different dependence of the forces on the particle volume is important, since one must ensure that magnetic forces dominate over other effects such as Brownian motion, gravitational forces or electrical forces between particles (a typical situation when using electrostatically stabilized particles). Detailed analysis of the interplay between all these possible forces under certain realistic situations can be found in the literature [40, 75]. Second, it is important to note that the effective force over a colloidal particle depends on the mismatch between the fluid magnetization and that of the particle. This allows for the manipulation of both magnetic and non-magnetic particles by tuning this magnetization mismatch. The controlled motion of non-magnetic particles is a phenomenon usually called *negative magnetophoresis*, since the magnetic force over the non-magnetic particle is in the opposite direction than the magnetic field gradient. In this situation, the effective magnetization of the fluid directs the motion of the particles immersed.

This controlled motion of magnetic particles using magnetic fields has been envisaged as a promising strategy in different medical applications. One of the first examples was proposed by Senyei *et al.* [76], who presented a new magnetic carrier microsphere for drug delivery. The main advantage in this approach is the possibility to avoid systemic drug distribution, reducing or even eliminating possible adverse side effects. They tested the performance of the new magnetic carriers proposed (an albumin matrix with Fe_3O_4 nanoparticles absorbed) by mimicking the real circulatory system in an *in vitro* setup. More recently, Yellen *et al.* [77] showed the controlled transport of non-magnetic particles (commercial fluorescent particles with sizes ranging between 90 nm and 5 μm) in a two dimensional arrangement of magnets immersed in an aqueous ferrofluid solution. The magnetic field was produced by several iron-core solenoids responsible to induce the magnetization of a lithographically patterned ferromagnetic substrate (70 nm thick cobalt thin film) into discrete patches. This template pattern, was used to produce reprogrammable inhomogeneous magnetic fields, leading to enhanced control over the assembly and manipulation of non-magnetic particles.

1.3.1 Magnetic separation

The aim of any separation process is to extract (separate) a desired component dispersed in solution out of the mixture. Over the years, magnetic separation has helped to face some problems related to separations in different technological areas, from industrial to laboratory applications. For instance, if part of a mixture is intrinsically magnetic, then magnetic separation often provides a higher throughput than equivalent centrifugation of filtration methods [78]. Thus, the use of this principle is straightforward in mixtures where a magnetic component is known to exist, as in the removal of tramp iron from different feed materials like kaolin clays or for the beneficiation[6] of ores since the beginning of the XX century [79–81]. Unfortunately, in some situations the target compounds in solution are non-magnetic, such as proteins or other molecules. In such cases, a typical strategy is the addition of magnetic colloidal particles (often called magnetic carriers) to the solution in order to catch and harvest the desired components. Typically, the magnetic carriers surface is decorated with proper functional chemical groups, designed to bind to the entities of interest. This strategy has been applied in very different areas, boosted by the improvement on the magnetic particle synthesis during the past 20 years. Nevertheless, this last approach has two main drawbacks. First, since the magnetic force acting on a magnetic particle is proportional to its magnetic dipole m, i.e., to its volume ($F_{mag} \quad m \quad d^3$), a faster separation is obtained by using particle with large magnetic moments; however, this would result in larger particles and hence one needs to balance this increase of particle size and the loss of surface/volume ratio. Second, sometimes one needs to unbind the magnetic particles from the target entities after the separation for their further reuse, since magnetic particles are usually an expensive component when compared to other colloidal particles used in separations like, for instance, latex colloids. This unbinding process is sometimes economically demanding and/or non feasible. Then, a third strategy intended to overcome some of the aforementioned drawback is the use of a magnetizable medium to direct the motion of the non-magnetic particles, called *negative magnetophoretic separation*. In this case, the motion of non-magnetic particles is controlled by tuning the mismatch between the magnetic response of the colloidal particles and that of the surrounding liquid.

---

[6] In mining, beneficiation is a variety of processes whereby extracted ore from mining is separated into mineral and gangue, the former suitable for further processing or direct use.

Thus, the key factors in any of such magnetic separation strategies are two: (i) the selection of appropriate particles with certain magnetic response and (ii) the design of adequate magnetic fields. Notice here that the magnetic field has not only to induce a net magnetization over the magnetic particles but also to generate a magnetic field gradient (the responsible for the magnetic force on the particle, Eq. 1.18) in order to drive carrier particles apart from solution. Then, the ideal conditions to be fulfilled by the magnetic field source are two: it has to induce large magnetizations but also a sufficiently intense magnetic field gradient. The simplest option to induce such a magnetic field in a lab tube or vial is by the application of a simple bar magnet (see Fig 1.12). However, this option can be highly inefficient because the magnetic field gradient is highly inhomogeneous in all the separation volume and particles far from the magnet experience smaller magnetic forces, thus slowing the overall separation process. Nevertheless, efficient magnetic separators are possible by arranging the magnets in certain configurations, generating more suitable magnetic fields and achieving efficient magnetophoretic conditions. The following sections are devoted to the description of three of the most widely used designs in magnetic separation.

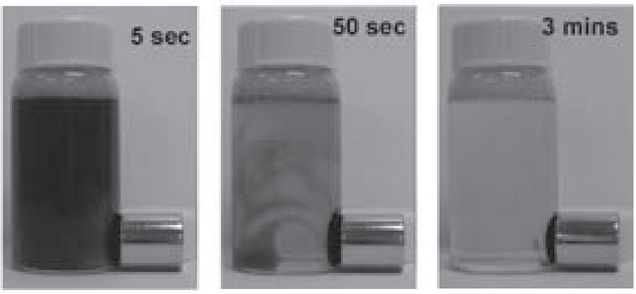

Figure 1.12: Real time-lapse images of the magnetic separation of Chlorella sp. by using 1000 mg L^{-1} TODA nanorods-PDDA by a NdFeB permanent magnet (extracted from [38]).

1.3.2 High Gradient Magnetic Separation: inhomogeneous conditions

As we have explained, the basic principle behind magnetic separation relies on the fact that materials with different magnetic moments experience different forces in the presence of magnetic field gradients. Originally, separation devices were designed to separate materials with high magnetic response as iron and magnetite, and the initial efforts were focused on the design of devices able to process a large variety of feed materials. The development of higher magnetic field gradients to trap smaller particles with small magnetic moments was also the object of many efforts. Fulfilling the requirements of large magnetic field gradients and large throughput, the first *High Gradient Magnetic Separator* (HGMS) was developed by Dr. Henry Kolm at the Francis Bitter National Magnet Laboratory at the late 60's, designed to face the problem of removing iron-stained titanium dioxide from kaolin clay [82]. The magnetic gradients generated by such devices were in the order of 1kOe/μm (10^5 T/m).

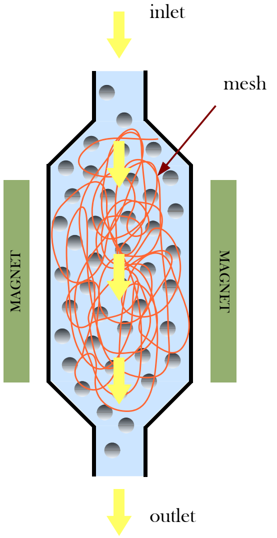

Figure 1.13: Sketch of a *High Gradient Magnetic Separation* device. The fluid containing the target magnetic particles is passed through the magnetized mesh (in red), which retains the magnetic particles of interest. After the separation is accomplished, the magnetic field is removed and the magnetic column is washed in order to recover the magnetic particles captured.

The HGMS concept is based on the fact that the magnetophoretic velocity of a magnetic particle is proportional to the magnetic gradient: since typical magnetophoretic velocities are very low, the key aspect is to develop systems with very high gradients. In order to generate these high magnetic gradients, the HGMS approach employs a column containing a packed bed of magnetically susceptible wires or fixed beads, which produce high local magnetic fields in their surroundings when an external magnetic field is applied (see Fig. 1.13). The suspension containing the magnetic particles is circulated along the column and the magnetic particles passing near the wires are captured by the high local magnetic fields. Typically, once the separation is accomplished, the separation column has to be washed in order to recover the magnetic particles. Due to the large magnetic gradients obtained at the surface of these beads or meshes, the HGMS devices are able to separate not only small ferromagnetic particles but also some other weakly paramagnetic materials (i.e. materials with much lower magnetic susceptibility when compared to a typical ferromagnet) [83, 84]. This new approach opened the possibility to apply the HGMS to a large variety of processes, from coal desulfurization [85], water pollution control [86, 87], clay beneficiation [88] or red blood cells separation [89]. Although the magnetic gradients achieved in these devices are really high, they are highly inhomogeneous. This hinders a detailed description of the separation process by theoretical models or simulations.

1.3.3 Precision Magnetic Separation: homogeneous conditions

As an alternative to HGMS, other approaches have been proposed to tackle the efficient magnetic separation of particles, for example *Precision Magnetic Separation* (PMS). In this approach, a uniform magnetic field gradient in the whole separation volume is achieved by arranging a set of permanent magnets in a quadrupolar-type geometry. An example of such devices are the magnetic separation devices from SEPMAG Technologies S.L. [90]. In Fig. 1.14 we present a sketch of their separator design and the monitoring system. In these devices, the magnetic field generated inside the separation volume is radially symmetric and its gradient points towards the cylindrical vessel wall. Moreover, the magnetic field gradient generated is approximately uniform along the whole separation volume, i.e. the magnetic field modulus increases linearly with the distance to the center of the separator, being approximately zero at the center. The initial dispersion contained in a bottle or test tube is placed in the separator, being the field gradient oriented perpendicular to the cylindrical walls. The radial magnetic force acting on each particle drives them toward the walls. The separation finishes when all the magnetic particles reach the wall of the container. At this stage, the particles can be easily recovered by pumping the clean solution with a syringe, keeping the particles inside the bottle. The separation process is easily monitored by measuring the amount of transmitted light through the sample by a rather simple and low-cost photodetector. For an easier visualization of the complete separation process we address to the movie available online [91].

The homogeneous magnetophoretic conditions obtained by adopting this strategy provides some advantages when compared to other separation technologies. For instance, the design of the magnetic field provides a more suitable framework to study the separation process by theoretical and/or simulation models as compared to HGMS-based devices or more simple arrangements of magnets. Interestingly, these separation

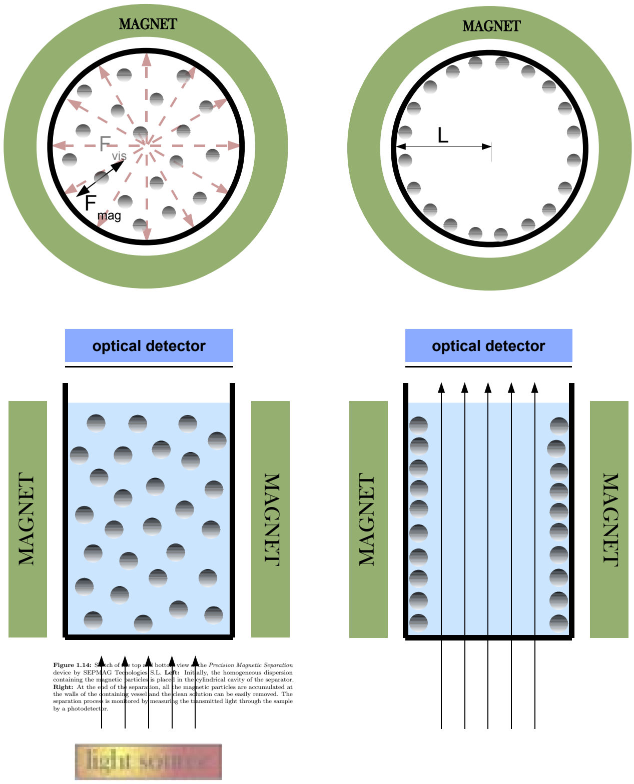
MAGNET
F_{vis}
F_{mag}
MAGNET
L
optical detector
optical detector
MAGNET
MAGNET
MAGNET
MAGNET
light source

Figure 1.14: Sketch of the top and bottom view of the *Precision Magnetic Separation* device by SEPMAG Tecnologies S.L. **Left:** Initially, the homogeneous dispersion containing the magnetic particles is placed in the cylindrical cavity of the separator. **Right:** At the end of the separation, all the magnetic particles are accumulated at the walls of the containing vessel and the clean solution can be easily removed. The separation process is monitored by measuring the transmitted light through the sample by a photodetector.

approach can be easily scaled up to deal with large volumes of solution, providing scalable separation processes. This is of special interest in biotechnological applications, for instance, as an alternative to centrifugation procedures or traditional fractionation columns. In addition, the PMS approach guarantees a better quality control thanks to the homogeneous working conditions.

Specially interesting were the experimental results obtained in recent experiments obtained by our group [51, 52], consisting in the separation of commercial superparamagnetic colloidal particles (M1-030/40 and M1-020/50 from Merck-Estapor) by using the Precision Magnetic Separation devices previously described. In those experiments it was observed that the separation time t_s depends significantly on the concentration c of the superparamagnetic colloidal particles in the dispersion:

$$t_s \sim c^{-\alpha} \tag{1.19}$$

with $\alpha \approx 0\ 25$. The fact that the separation time t_s depends on the concentration (which was unexpected according to previous magnetophoretic separation studies) implies that the motion of the colloids during the separation process is dominated by a collective behavior rather by the individual motion of each colloid. This dependence on the concentration indicates that the collective behavior is also a cooperative one, which speeds up the separation. Indeed, if one ignores the interaction between colloids, a simple calculation predicts separation times several orders of magnitude longer than the observed ones. Direct observations of the separation process under a microscope show that after the application of the external magnetic field, linear aggregates (chains and bundles) of colloids are build up along the field direction and move in the direction of the magnetic gradient. After removal of the external field, the aggregates break up and the original dispersion is recovered, thanks to the superparamagnetic character of the colloids (see section 1.2.1). These results show that the mechanism behind this fast magnetic separation is the reversible aggregation of the magnetic colloids induced by the external field. Therefore, one must distinguish between this *cooperative magnetophoresis*, where aggregates form leading to shorter separation times, and *non-cooperative magnetophoresis*, in which each particle moves as a single entity.

1.3.4 Microfluidics Separation Devices

A different approach to target the separation of particles from solution has emerged thanks to the miniaturization of lab technology, mainly focused on small volume samples with high biotechnological interest. The coupling of microfluidic devices and magnetic fields has lead to different strategies for particle separation and fractionation [92–94]. One of the most extended methodologies which couples the magnetic fields to nanofluidic devices is the *Free-Flow Magnetic Separation* (FFMS). In this approach, a magnetic field gradient perpendicular to the fluid flow direction is created by surrounding the microchannel by certain arrangement of magnets. This configuration has been proven to effectively deflect the magnetic particles from the fluid flow, separating them from the initial dispersion [95].

In a typical microfluidic device, the channel is a few centimeters long and half millimeter wide (Fig. 1.15). The small magnets situated at the walls attract the magnetic colloids dispersed in the flowing liquid, which are eventually deflected or immobilized onto the walls. Controlling the deflection of the magnetic particles opens the possibility to separate particles with different size and/or magnetic response, as shown in different multiplexed systems [67, 96, 97]. If the functionalized magnetic colloids are immobilized onto the walls, they act as a functionalization of the microfluidic channels and are able to capture dissolved species into the flowing liquid. After the capture of the desired entities, the magnetic colloids can be released as desired by deactivating the magnetic field and recovered for their reuse.

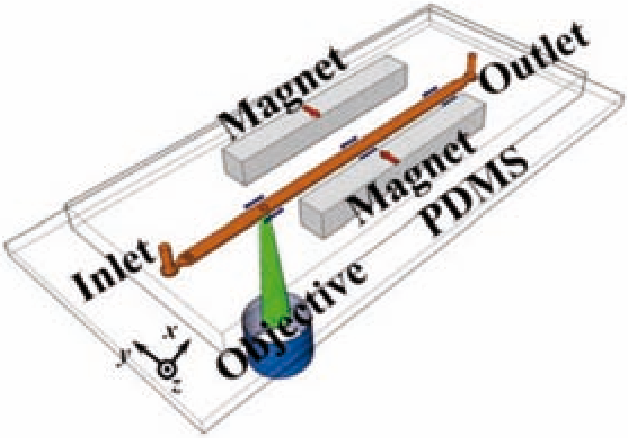

Figure 1.15: Sketch of a typical nanofluidic device. The standard strategy in nanofluidic devices is the deflection of the trajectories of the particles by generating a magnetic field gradient inside the microfluidic channel perpendicular to the fluid direction.

For instance, Beveridge reported the purification and separation of magnetic nanoparticles ($CoFe_2O_4$) mixtures using *Differential Magnetic Catch and Release* (DMCR) technique [98]. In this method, a variable magnetic flux is applied perpendicular to the flow direction. They showed that, balancing the relative strength of the drag and magnetic forces, particles with sizes in the range 8-17 nm can be efficiently separated. The negative magnetophoresis concept has also been applied in nanofluidic devices. Zhu *et al.* reported experiments of the fractionation of non-magnetic particles together with an analytical model to describe the separation process [99, 100]. Despite the rather simple description, they optimized the device, accounting for important properties like particle size, ferrofluid properties, magnetic field distribution and fluid flow rate. Thanks to these improvements, they also showed the possibility to focus the particles inside the microchannel device forming a thin flux column inside the nanodevice [101].

The potential of such approach was demonstrated by separating cells by negative magnetophoresis, showing the large potential of such technologies readily applicable in bioassays [102].

1.4 Simulation Techniques

Computer Simulations is a mature approach widely used in a variety of research areas and engineering, providing a theoretical framework to study from ideal systems and fundamental theories to more realistic models of real systems. For instance, through computer simulations one can gain access to some system properties unavailable from experimental techniques or provide numerical solutions to problems which could not be addressed otherwise, being a complementary tool to theory and experiments. Different simulation techniques have been developed along the years, and the increase in computing power has boosted the extension of computer simulations to many different fields. The different simulation techniques are usually classified according to the time and length scales of the physical phenomenon of interest which they can describe. A basic scheme showing the different simulation techniques according to the time and length resolution is provided in Fig. 1.16. According to the different phenomena of magnetic colloidal dispersions (aggregation, growth kinetics and magnetophoresis) described along the introduction, and according to the hierarchy scheme proposed, mesoscale simulation methods seem to be the most suitable approach to address those issues.

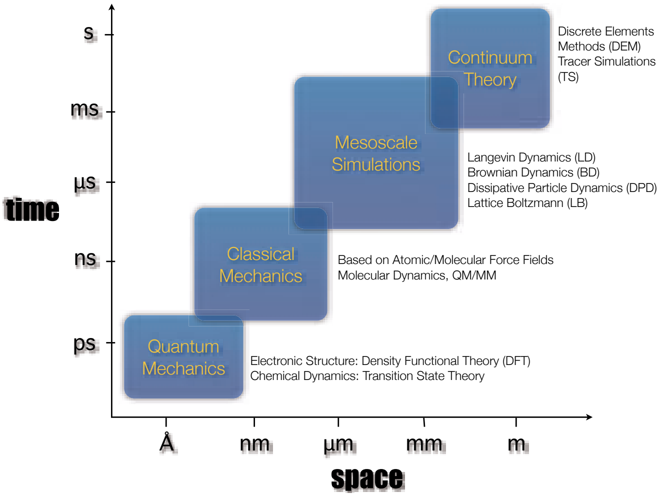
s
ms
µs
time
ns
ps
Continuum Theory
Discrete Elements Methods (DEM)
Tracer Simulations (TS)
Mesoscale Simulations
Langevin Dynamics (LD)
Brownian Dynamics (BD)
Dissipative Particle Dynamics (DPD)
Lattice Boltzmann (LB)
Classical Mechanics
Based on Atomic/Molecular Force Fields
Molecular Dynamics, QM/MM
Quantum Mechanics
Electronic Structure: Density Functional Theory (DFT)
Chemical Dynamics: Transition State Theory
Å
nm
µm
mm
m
space

Figure 1.16: Diagram showing the different simulation and computational techniques according to the relevant length and time scales of the processes which they can describe.

In statistical physics, the Langevin stochastic differential equation describes the time evolution of a subset of the degrees of freedom. These degrees of freedom are typically separated in two different sets, one collective set (macroscopic) of variables changing only slowly in comparison to the other set (microscopic) of variables of the system. For instance, this formalism can be used to describe, from a mesoscale framework, the dynamics of the colloidal particles immersed in a fluid. In this situation, the dynamical properties of the colloids are solved explicitly while the fluid molecules are treated implicitly, defined as a continuum medium where hydrodynamic effects and thermal fluctuations are included. In this manner, in *Langevin Dynamics simulations*, the equation governing the dynamics of a single colloidal particle of mass m can be written as:

$$m\frac{d^2r}{dt^2} = F_f + F_r + F_c \tag{1.20}$$

In this equation, the force F_f is the viscous resistance experienced by the colloid due to the surrounding fluid, and in its simple version, is proportional to the velocity of the colloid v as given by the Stokes formula:

$$F_f = -3\pi\eta d v = -\frac{m}{\tau}v \tag{1.21}$$

where d is the diameter of the colloidal particle and η is the viscosity of the solvent. The so-called damping parameter τ is given by:

$$\tau = \frac{m}{3\pi\eta d} \tag{1.22}$$

and it has units of time. This damping parameter gives the typical timescale for the relaxation of the colloid to a stationary state with velocity $v = (\tau \;\; m)F_c$, where the term F_c includes all different interactions between colloidal particles (dipolar magnetic forces, electrostatic interactions, van der Waals forces, etc...) and/or external forces. The F_r contribution accounts for the collisions between solvent molecules and colloidal particles. It is an stochastic or random force corresponding to a white noise (i.e. its variations are extremely fast compared to the changes of the colloid's velocity) with zero average and obeying the fluctuation-dissipation theorem:

$$F_r(t) \cdot F_r(t') \;\; = 2k_BT\frac{m}{\tau}\delta(t-t') \tag{1.23}$$

where T is the temperature of the system. The implementation of this approach applied to many particle systems is available in several standard simulation software packages [103, 104].

In *Brownian Dynamics* $t \gg \tau$ and one can consider that the velocity of the colloidal particles has relaxed to its equilibrium distribution (Maxwell distribution). Thus, if no external forces are present, the average displacement of the particles is zero and the fluctuations in particle positions obey the diffusive relation:

$$r^2(t) \;\; = 6Dt \tag{1.24}$$

where D is the diffusion coefficient of the colloidal particle given by the Einstein relation:

$$D = \frac{k_B T}{3\pi\eta d} \tag{1.25}$$

The Brownian Dynamics approach is sometimes referred as "overdamped" Langevin Dynamics or as Langevin Dynamics without inertia. More detailed discussions on these methodologies can be found in literature [105].

Different implementations of the Brownian Dynamics approach are available, being the one from Ermak and McCammon the most widely adopted [106]. In that scheme, the motion of every particle in the simulation is calculated at each time step as the sum of two different contributions. A deterministic term arising from the interaction between particles and/or external fields, and a random term which accounts for the thermal fluctuations in the system, and it is related to the diffusion of the particle in the given solvent. This random term is calculated by generating a random displacement of each single particle following a gaussian distribution. In absence of the deterministic term, the random motion generated recovers the diffusion coefficient, according to the diffusive relation given in Eq. 1.24.

Such Brownian Dynamics simulations have been applied to face the magnetophoretic separation as in the work by Schaller *et al.* [56]. They reported a complete experimental and theoretical work on the magnetophoresis of nanometer size nanoparticles (ranging from 50 nm up to 425 nm in size) under the effects of a magnetic gradient. They stated that a non-interaction particle model does not suffice to account for the short separation times observed in those systems. They claim that the formation of chains is the responsible of the short separation times obtained. Nevertheless, they also argue that the separation time depends only marginally on the colloid concentration, a fact which is in contradiction with similar experiments realized in our group [52].

Nevertheless, other methods to describe the motion of colloidal particles in liquids exist apart from Langevin and Brownian Dynamics. For instance, it is known that the diffusion coefficient (Eq.1.25) is not constant and that can be affected by hydrodynamic interactions between colloidal particles. To account for such interactions, other simulation methodologies arise as alternatives to Langevin or Brownian Dynamics, like Lattice Boltzmann simulations, which have been recently used in simulations of ferrofluid dispersions [107].

In a different view, sometimes one does not need more detail in the simulation method, but rather a simple description of the phenomena of interest. Under this circumstance, one should move towards continuum computational methods (Fig. 1.16), such as *Finite Element* methods or *Particle Tracers* simulations. For instance, in Particle Tracer simulations each particle (or tracer) is not intended to represent a real particle but it effectively describes the dynamics of a given particle under the external conditions imposed (a particle tracer can be seen as a buoy used to track the see level, instead of following the individual motion of a single water molecule at the sea surface). Particle Tracer simulations are commonly used in fields such as fluid mechanics to describe situations in which the particles follow a ballistic motion rather than being dominated by brownian diffusion [108].

1.5 Motivation & Scope

In view of the issues exposed along this chapter, the motivation and aims of this thesis work can be summarized in two blocks. As we have seen, different structures can emerge in superparamagnetic colloidal dispersions under the effects of uniform magnetic fields, and these structures can become even more complex by using mixtures of particles with different magnetic response or by tuning the magnetization of the medium (see Figs. 1.10 and 1.11). Nevertheless, some deeper understanding of the relation between the physical parameters controlling the system and the emerging structures is desired. In particular, it is not clear which are the threshold values of the volume fraction π_0 and magnetic strength Γ required to guarantee the initial formation of superparamagnetic chains, nor the existence of equilibrium situations in which these structures remain unchanged. Besides, the kinetic laws directing the growth of such structures or the mechanism behind their evolution to much complex entities (like bundles or fibers) remain not clear. A second area of open questions is the paradigmatic example of the magnetic separation. Although it has been a standard approach used in many different applications, there is still a poor understanding about the basic mechanisms.

The development of new modeling tools may help to boost the rational study of superparamagnetic colloidal systems, providing realistic models representative of experimental situations. These tools should improve the agreement between experimental results and theoretical predictions, and enlarge their applicability to the vast variety of research areas in which superparamagnetic nanoparticles are used. Furthermore, they should also provide methodologies able to predict the magnetophoretic velocities as a function of particle properties and the applied magnetic field gradients.

Those issues have motivated our research, searching for new theoretical approaches and simulation tools, and the results obtained are presented separately in two chapters. In Chapter 2 we have summarized the detailed objectives and results corresponding to aggregation phenomena in superparamagnetic dispersions under homogeneous magnetic fields. And Chapter 3 has been devoted to present the main objectives and the corresponding results obtained in the study of different magnetophoretic processes under uniform magnetic field gradients. All these results have been published in international peer-reviewed journals, and the corresponding articles are appended in Chapter 4.

Chapter 2

Results I: Chain formation under uniform magnetic fields

In this chapter we present the results corresponding to aggregation phenomena in superparamagnetic colloidal dispersions under uniform magnetic fields. The results summarized here have been published in the following articles:

> **Article 1:** "Aggregation of superparamagnetic colloids in magnetic fields: the quest for the equilibrium state", *Soft Matter* **7**, 2336 (2011).
>
> **Article 2:** "*On-the-fly* coarse-graining methodology for the simulation of chain formation of superparamagnetic colloids in strong magnetic fields", *Physical Review E* **85**, 036709 (2012).

2.1 Objectives

1. Establish an aggregation criterion to predict the chaining process arising in superparamagnetic colloidal dispersions under certain conditions.
2. Study the different kinetic regimes as a function of the volume fraction of superparamagnetic colloids, π_0, and the characteristic magnetic strength parameter, Γ.
3. Set up a new simulation model specially designed to study the aggregation kinetics of superparamagnetic colloidal dispersions, in view of the difficulties encountered to reach larger time and length scales with Langevin Dynamics simulations.

2.2 Summary

Colloidal aggregation is a subject of active research for both practical and fundamental interest: from stability of many industrial products to a test field for statistical-mechanics theories. Our interest here resides in the new physics arising in the aggregation behavior of superparamagnetic colloidal dispersions. It is well know that these aggregation phenomena have important consequences in the physical properties of such colloidal systems and they have special relevance in different research areas, like magnetic separation [51,52], magnetic particle imaging [3,43,109] or magnetic colloidal crystals [19, 31, 110].

Previous experimental studies of superparamagnetic colloidal dispersions under strong magnetic fields have shown the formation of different structures (see Fig. 1.10). Here we will perform Langevin Dynamics simulations to systematically study the aggregation phenomena, mentioned in sections 1.2.2 and 1.2.3, by selecting different values of Γ and π_0. We have defined three different aggregation regimes, no aggregation, equilibrium state and irreversible chain growth. We have also provided an analytical expression to calculate the mean number of particles in a chain N in equilibrium on the basis of a thermodynamical model.

We have found some difficulties when modeling real experimental situations involving superparamagnetic colloids by Langevin Dynamics simulation, like in the T_2 relaxation time measurement of water protons in superparamagnetic dispersions [43, 44] or the *cooperative* magnetophoresis separation [7, 51, 52]. When modeling such processes by computer simulations, one needs to consider microscopic time and length scales but also reach macroscopic time scales at low computational cost. To do so, we have introduced a new methodology based on an *on-the-fly* Coarse-Grain (CG) model. In our new approach, the coarse-grain objects in the simulation and their dynamic behavior are not fixed *a priori* at the beginning of the simulation but rather redefined *on-the-fly*. With this model, we have been able to tackle the description of the irreversible chain formation observed in dispersions of superparamagnetic colloids.

2.3 Results

2.3.1 Aggregation kinetics and equilibrium state

The superparamagnetic colloidal dispersions studied in this work are described by two characteristic parameters: the magnetic strength Γ (Eq. 1.11) and the initial volume fraction of colloids π_0 (Eq. 1.13). We have chosen values in the range $\Gamma = 3 - 40$ and $\pi_0 = 5\ 23 \times 10^{-3} - 5\ 23 \times 10^{-4}$ since they are representative of real experimental conditions.

In the Langevin Dynamics simulations presented in this chapter, each superparamagnetic colloid has equal diameter, mass and magnetic moment and it is represented by a soft sphere through a 6-12 Lennard-Jones potential. We have assumed the particles to be in the saturation regime i.e. the magnetic field applied is large enough to bring the magnetization of the particles up to its saturation value. In this situation, the magnetic moment of each particle points along the magnetic field direction and remains constant (in magnitude and direction) during the simulation. The magnetic dipole-dipole interaction is calculated explicitly and solvent and thermal effects are included in the Langevin stochastic equation of motion, characterized by the viscosity of the solvent at the given temperature (see description in section 1.4). All simulations have been carried out using the same simulation software (LAMMPS, version 21May2008 [104]).

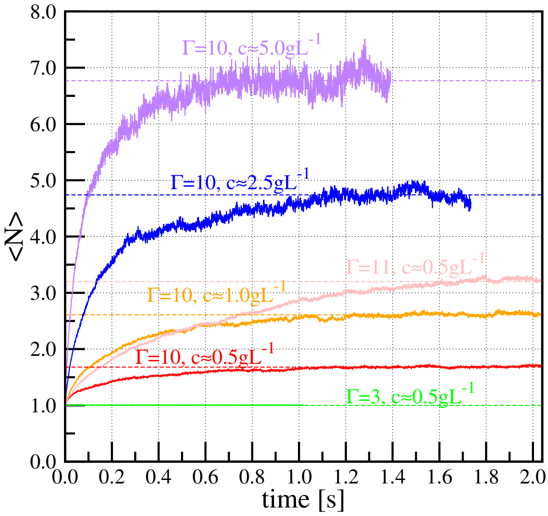

Figure 2.1: Time evolution of the average chain length $\langle N\rangle$ in Langevin Simulations with different values of Γ and different concentrations. Dashed lines indicate the average chain length $\langle N\rangle$ reached at equilibrium, calculated by averaging over the last 0.5 s of each simulation. This figure summarizes the simulation results shown in figures 2 and 3 from article 1.

In Fig. 2.1 we show the computed average chain length N as a function of time for different systems obtained from our simulations. In this figure, two aggregation regimes can be observed. The simulation with the lowest value of the magnetic strength parameter ($\Gamma = 3$) and a volume fraction of $\pi_0 = 5\ 23 \times 10^{-4}$ (equivalent to a concentration of 0.5 gL^{-1}) shows no significant aggregation. This indicates that the superparamagnetic dispersion remains unchanged after the application of the magnetic field, even when the magnetic interaction energy exceeds the characteristic thermal energy of the system. This contrast with the classical criterion [49], which considers that aggregation arises for values $\lambda > 1$. For larger values of the magnetic strength (for instance, for $\Gamma = 10$) and the same volume fraction as in the previous case, the particles start to aggregate. After a fast transient regime, the average chain length N reaches different equilibrium values, depending on the intensity of the magnetic strength and the volume fraction of the system. Larger concentrations of colloids translate to larger values of the average chain length N , as it is shown for $\Gamma = 10$ and 4 different concentrations. Following a similar behavior, larger values for the average chain length are also achieved by increasing the magnetic interaction parameter Γ and a constant volume fraction $\pi_0 = 5\ 23 \times 10^{-4}$, as it is shown for the case $\Gamma = 11$. We notice here that these were the first simulation results showing the existence of this equilibrium state in superparamagnetic dispersions but they could not be compared to existent theoretical models [47], aimed to describe ferrofluid dispersions.

In view of these results, we considered the application of a simple thermodynamic calculation based on self-assembly theory [111] in order to describe the dependence of the average chain length with Γ and π_0. The model we proposed considers an ideal solution of superparamagnetic colloidal particles under an external magnetic field together with a mean field approach to evaluate the interaction energy between colloidal particles inside a chain. This situation is similar to the model presented by Ivanov *et al.* [112], which was intended to describe the aggregation process in dispersions of permanent dipolar particles in absence of external magnetic fields. In our approximation, the chemical potential μ_s of a colloid forming part of a chain of s colloids is given by the ideal (entropic) term plus the interaction energy term, which accounts for the $s - 1$ bonds between the colloids forming the chain:

$$\mu_s = \mu^0 + \frac{1}{s}\left[k_B T \ln \frac{\pi_s}{s} - (s-1)\ _m\right] \tag{2.1}$$

where π_s is the volume fraction of chains containing s colloids and $_m$ is the magnetic interaction energy between two colloids in contact and with their magnetic dipole aligned with the magnetic field direction. In the equilibrium situation, μ_s are equal (independently of the length s of the chain) and we can obtain the distribution of chains of length s.

The strength of the magnetic bond between colloids in a chain can be calculated by considering the thermal average of the interaction between two colloids in contact over all possible relative orientations, being $\beta \quad = \Gamma - 1$ (see equation 8 in article 1, for a detailed derivation). The results can be expressed as a function of the *aggregation parameter*, N^*, defined as:

$$N^* = \quad \overline{\pi_0 e^{(\Gamma-1)}} \tag{2.2}$$

For $N^* \ll 1$, which corresponds to very dilute systems or very low magnetic coupling parameter, no significant aggregation is expected and the average chain length becomes $N \quad = 1$. In the opposite case, for $N^* \gg 1$, the number of chains of length s per unit volume, n_s, is given by:

$$n_s \quad \pi_s \ s \approx (1 - 1\ N^*)^s \approx e^{-s/N^*} \tag{2.3}$$

and then, we can approximate $N \quad \approx N^*$. In sight of these results, we can state that Eq. 2.2 provides, not only a criterion to predict when the aggregation process will appear in superparamagnetic dispersions, but also to estimate the average chain length at equilibrium. In Fig. 2.2 we compare the average chain length obtained from the Langevin Dynamics simulations N (corresponding to the simulations presented in Fig. 2.1) and the corresponding aggregation parameter N^*. The agreement between the simulations and the thermodynamical model is remarkably good in this range of parameters, showing only small discrepancies. The criterion defined by Eq. 2.2 has been applied to different experimental systems with satisfactory results [7]. Important to notice here is that, when applying Eq. 2.2 in real situations, one should also keep in mind that this analysis is only valid provided that N^* is much smaller than the initial number of colloids in the sample.

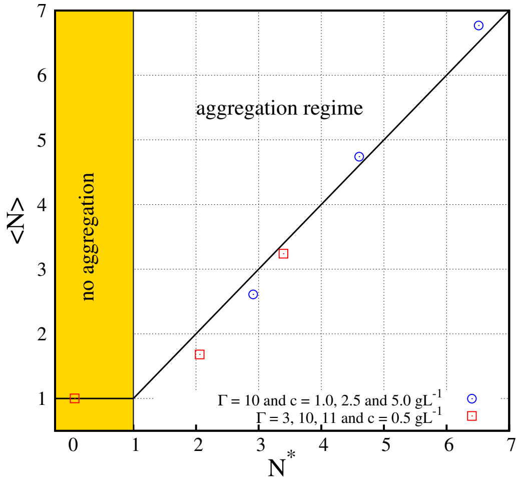

Figure 2.2: Average number of particles in a chain $< N >$ in the equilibrium state of superparamagnetic colloids under a strong field as obtained from simulations at different values of the aggregation parameter N^* defined by Eq.2.2. The simulations correspond to different values of the magnetic coupling parameter Γ and the volume fraction ϕ_0. The predicted no aggregation ($N^* \leq 1$) and aggregation ($N^* > 1$) regimes are indicated. The solid line corresponds to the prediction of Eq. 2.2 for the equilibrium size of chains in the aggregation regime (results adapted from article 1).

However, Eq. 2.2 does not provide any information about the time required to reach this equilibrium state. Notice that for slightly larger values of Γ the average chain length N becomes extremely large. For instance, for a volume fraction $\pi_0 = 5\ 23 \times 10^{-4}$ and $\Gamma = 25$, Eq. 2.2 gives $N^* = 25$, and for $\Gamma = 40$ this value is approximately $N^* \sim 6\ 7 \times 10^6$. In Fig. 2.3 we show the simulation results for both systems up to 2 s. We observe that in these simulations, and after an initial transient regime, the chain formation follows a power-law behavior (as mentioned in section 1.2.3). Combining the average chain length predicted by the thermodynamical model for the equilibrium situation and the power-law behavior observed (with an exponent value approximately $z = 0\ 64$), we can roughly estimate the required time to reach the equilibrium state for both systems, being $\sim$ 10 s and $\sim$ 10 years, respectively. Thus, we conclude that even when a well defined equilibrium state exists according to the thermodynamical model presented, this state is not always accessible.

At this point, it should be noted that the experimental window of parameters Γ and π_0 in which the equilibrium state should be observable is quite narrow. In fact, the vast majority of experimental reports of superparamagnetic dispersions under magnetic fields correspond to the case of continuous growth of aggregates and a few experiments correspond to the case of no aggregation. An experimental study reporting observations of the equilibrium state by optical microscopy was reported in Ref [62] but for the case of a bidimensional system, so direct comparison with our predictions is not possible. More recently, Barret *et al.* [113] observed an equilibrium state for concentrated superparamagnetic dispersions, employing neutron scattering techniques. In this case, their conditions (high volume fraction) are typical of ferrofluids and make very difficult analytical predictions. At this point, it should be emphasized that an early ferrofluid model of Pincus and de Gennes [47] predicted the existence of an equilibrium state. However, their model was unable to capture the behavior observed in our simulations, particularly the behavior observed in Figure 2.2 and the role of the aggregation parameter N^*.

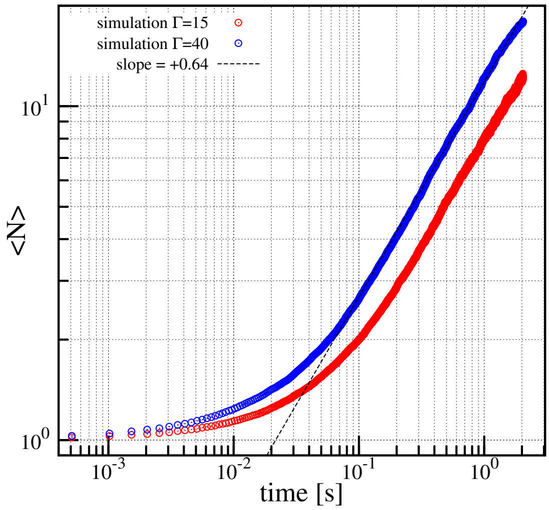

Figure 2.3: Time evolution of the average length of chains in simulations with concentration ~ 0.5 gL^{-1} ($\phi_0 = 5.23 \times 10^{-4}$) and magnetic strength parameter $\Gamma = 15$ and 40. The dashed line corresponds to a power-law fit of the form $\langle N \rangle \sim t^z$ for the case of $\Gamma = 40$. Figure extracted from article1, figure 1.

This kinetic aggregation regime observed in systems with large values of Γ is in agreement with previous studies on the aggregation kinetics in magnetic colloids. Experimental results and computer simulations of different cluster-cluster aggregation models showed that the behavior of different quantities such the average chain length N or the mass aggregate size S (defined in Eqs. 1.15 and 1.17, respectively) follow a power law behavior [50, 53, 71, 114, 115]. For instance, the average chain length, N , follows a power-law of the form mentioned in Eq. 1.16. In general, the dynamic exponent z depends on the dimension of the space as well as on the nature of the aggregation process. Our simulation results are consistent with previous results, in which kinetic exponents reported are in the range $z = 0\ 6 - 0\ 7$ [50, 53, 71].

However, we realize that the use of Langevin Dynamics simulations is too costly to face the aggregation dynamics in such systems. For example, the cost to achieve simulation runs as long as 2s was in the range of thousands of hours in CPU time (more details on the computational cost can be found in article 1). The main difficulty encountered in these simulations is that the continuous formation of chains increases the number of dipolar interactions that one has to account for at each timestep. In addition, the motion of a given aggregate is the result of the collective motion of each individual particle inside the aggregate. Clearly, the resolution of the motion of each individual particle inside an aggregate is not necessary if one is only interested on the irreversible aggregation kinetics. Thus, a different approach may be adopted to overcome the long time required to calculate the magnetic dipole-dipole interactions between particles inside a chain. In order to avoid such costly calculations, a new simulation scheme was proposed on the basis of these requirements and it is presented in the following section.

2.3.2 Irreversible chain growth

In this part, we have focused our attention in situations (fixed by π_0 and Γ) in which the external magnetic field induces the formation of linear chains of colloids which grow irreversibly with time or, in other words, in situations in which the aggregation parameter is very large ($N^* \gg 1$). In order to retain the underlying physics of the irreversible chain growth (showed in Fig. 2.3), we need to consider: *i)* the diffusive motion of particles and chains, and *ii)* their respective magnetic and steric interactions. Thus, our Coarse-Grain model ignores some details of the particles forming the chains: we replace the individual motion of the colloids in a chain by the motion of the chain as a single entity, and we also replace the actual magnetic dipole-dipole interaction by an effective short-range interaction, much less demanding from the computational point of view. An sketch showing these simplifications is provided in Fig. 2.4.

The first ingredient of the model is the description of the diffusion of each CG object (single particles and aggregates) in the simulation. For this purpose, we have adopted an anisotropic diffusion model proposed in the framework of slender body theory [116] which accounts for the elongated shape of the chains. In this model, the diffusion is represented by two different diffusion coefficients: one corresponding to the direction parallel to the symmetry axis of the object $D^{\parallel}$ and a second coefficient corresponding to the perpendicular diffusion $D^{\perp}$ (see Figs. 2.4, panels a and b). This diffusive motion of the CG objects is implemented in our simulations using a typical Brownian Dynamics scheme [106].

The second ingredient of the model is the definition of the effective interaction

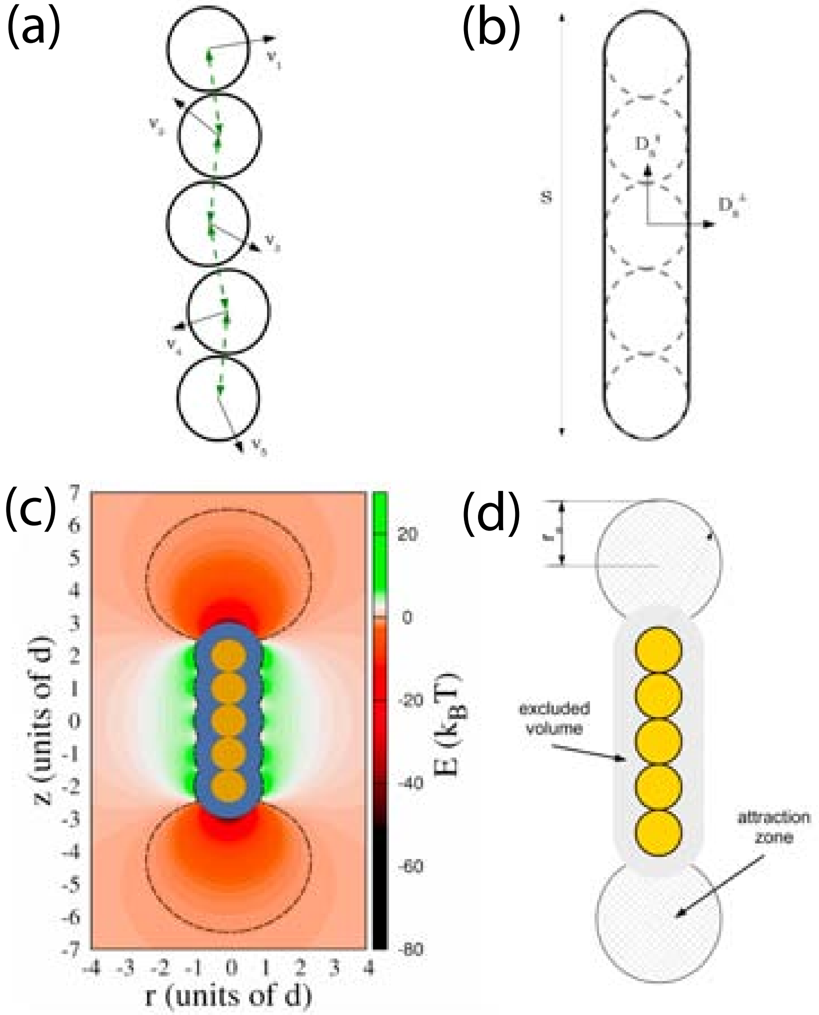
(a)
v1
v2
v3
v4
v5
(b)
S
Ds∥
Ds⊥
(c)
z (units of d)
7
6
5
4
3
2
1
0
-1
-2
-3
-4
-5
-6
-7
-4 -3 -2 -1 0 1 2 3 4
r (units of d)
20
0
-20
-40
-60
-80
E (kBT)
(d)
ra
excluded volume
attraction zone

Figure 2.4: **(a)** In Langevin Dynamics simulations, the motion of each individual colloid is calculated at each timestep and the stability of the chain results from the dipolar interactions between colloids in the chain. **(b)** In the Coarse-Grain approach, the motion of each coarse-grain object is calculated through the diffusion coefficients of the anisotropic model ($D^{\perp}$ and $D^{\|}$), rather than through the motion of each individual particle forming the chain. **(c)** 2D-map corresponding to the interaction energy between an incoming test dipolar particle and a chain-like aggregate formed by five colloids with magnetic strength parameter of $\Gamma = 40$. The black dashed line limits the region where $E \leq -k_B T$ and the blue region is the excluded volume, not accessible by other colloids. **(d)** Sketch of the interaction model implemented in our code. Each CG object has two attraction zones, modeled as a sphere of radius r_a tangent to the edge of the aggregate. Any object entering into these zones will immediately aggregate forming a longer chain. This figure has been adapted from figure 1 in article 2.

between CG objects. To this end, we have replaced the actual dipole-dipole magnetic interaction between colloids by an effective, short-range interaction between CG objects and an aggregation criterion (Fig. 2.4, panels *c* and *d*). For each CG object, we have defined two spherical attractive regions of radius r_a located at the two ends of the chain. These regions were designed to mimic the region at which the magnetic attraction between a chain of s particles and an incoming test dipolar particle is equal or stronger than the thermal energy. In this situation, we assume that when a given CG object enters any of those attraction regions belonging to another object, both CG objects are merged into a single object. If the two objects collide but there is no overlap with the aggregation regions, they will keep moving as independent entities (see figure 2 from article 2 for a description of the collision scheme adopted). With this approach, the chain formation process is irreversible in the sense that chains cannot disaggregate into smaller objects during the simulation.

The new model proposed was compared against standard Langevin Dynamics simulations. We compared results for a variety of systems, in a wide range of volume fractions and values of the magnetic strength [44, 117]. The volume fractions and the magnetic strength were in the range $\pi_0 \sim 10^{-4} - 10^{-6}$, $\Gamma \sim 40 - 247$ respectively, since the typical irreversible growth was expected in this range. With this new methodology, we have obtained results in good agreement with previous Langevin Dynamics simulations. In Fig. 2.5 we show a comparison between the average chain length $\langle N(t) \rangle$ obtained in both simulation approaches. As it can be observed, there is an excellent agreement between both methodologies in spite of the simplifications made in the new approach. Moreover, this agreement has been also confirmed by comparing the probability distribution of aggregates of different size $p(s;t)$ (see figures 5 and 6 in article 2.)

In order to ensure the robustness of our approach, we have also evaluated different options in the simplifications used in our approach. For instance, we have performed simulations with a different anisotropic diffusion model proposed by Tirado *et al.* [118] as an alternative to the slender body theory description. We could not find any significant difference between the results obtained with both models and hence, we decided to keep the slender body theory model based on its major simplicity (see figure 8 in article 2 for more details). In the other hand, we also showed how the increase in the size of the aggregation zones as a function of the aggregate length is crucial to recover the behavior found in Langevin Simulations, specially in the fast initial aggregation regime (as it is shown in figure 9 from article 2).

From a more technical point of view, we have also compared the performance of both simulation approaches for different systems and the corresponding results are summarized in Tab. 2.1. We can see that the reduction on the required CPU time is very large. For instance, in the case of $\Gamma = 40$, the new Coarse-Grain approach achieves the end of the simulation (5 s) in only 25 hours, while the required CPU time to achieve half the simulated time for the same system is approximatively 40 times larger in the Langevin Dynamics simulations. Further details of the CPU time required in both simulation methodologies are provided in article 2, tables 2 and 3.

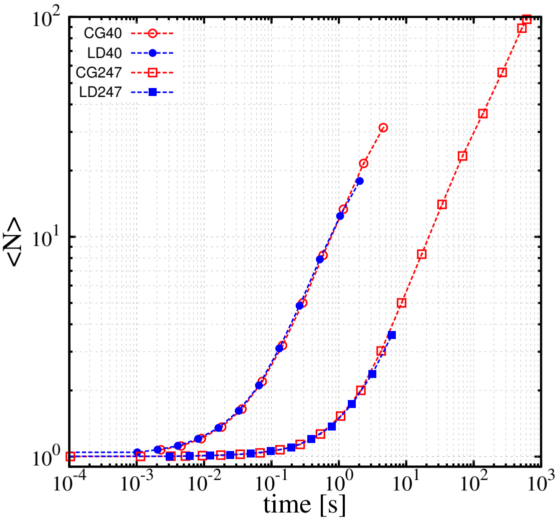

Figure 2.5: Time evolution of the average chain length $\langle N(t)\rangle$. Comparison between the results obtained from Langevin Dynamics simulations (solid symbols) and Coarse-Grain simulations (open symbols) for the two different systems studied. Circles correspond to case $\Gamma = 40, \phi_0 = 5.23 \times 10^{-4}$ and squares to case $\Gamma = 247, \phi_0 = 4.64 \times 10^{-6}$. This plot corresponds to figure 4 in article 2.

Table 2.1: Comparison of the performance between Langevin Dynamics and the Coarse-Grain model proposed for different systems. The Δt is the timestep used in each integration scheme and t_f is the total simulated time. We have also indicated the total amount of CPU cost for each single run, calculated as the number of cores used multiplied by the total elapsed time. In all our calculations we have used a 8-Core AMD Opteron Magny-Cours 6136 processor. Table adapted from table 2 in article 2.

Label	Δt [s]	t_f [s]	# cores	CPU cost
LD40	1.02×10^{-9}	2.04	8	998h
LD247	3.06×10^{-9}	6.12	8	866h
CG40	$2\,280 \times 10^{-4}$	5	1	25h
CG247	$1\,038 \times 10^{-4}$	1000	1	24h

Finally we have illustrated the application of this new model to an experimental situation, namely the measurement of the transverse relaxation time T_2 of water protons in dispersions of superparamagnetic nanoparticles [43, 44]. It is known that the aggregation in such dispersions modifies this relaxation time. As proposed in reference [44], we can estimate the time evolution of the relaxation rate $1/T_2$ from our simulation results by computing the average:

$$\frac{1}{T_2(t)} = \frac{1}{N_p} \sum_s s n_s(t) \frac{1}{T_2^{(s)}} \tag{2.4}$$

where $1/T_2^{(s)}$ is the relaxation rate of water protons near a colloid forming part of a chain containing exactly s colloids and $n_s(t)$ is the number of chains of size s at time t. The simulations have shown a remarkable agreement between theory and experiments for times corresponding to average chain length up to 50 colloids (Fig. 2.6).

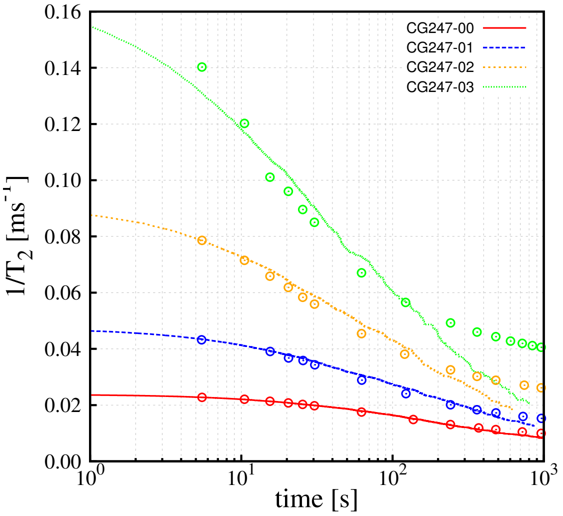

Figure 2.6: Evolution of the relaxation rate $1/\mathrm{T}_2$ of water protons in four dispersions characterized by $\Gamma = 247$ and containing different concentrations of superparamagnetic colloids $\phi_0^{(00)} = 1.16 \times 10^{-6} = 8\phi_0^{(03)} = 4\phi_0^{(02)} = 2\phi_0^{(01)}$. Solid lines correspond to the predictions obtained from Coarse-Grain simulations and symbols correspond to experimental data. These results correspond to figure 11 in article 2.

2.4 Conclusions

- We have shown by employing Langevin Dynamics simulations the existence of different aggregation kinetics under the effects of an external magnetic field. A first regime, found for low values of Γ and relatively low concentrations, in which the superparamagnetic dispersions remain in the same initial state (no chains are formed). A second regime, corresponding to low volume fractions and values of $\Gamma < 15$, in which it is observed that, after a transient period of chain formation, the system attains an equilibrium state. The existence of such an equilibrium state was reported, for the first time, in the basis of computer simulations. Finally, a third regime, corresponding to cases with $\Gamma > 15$, in which our Langevin Dynamics simulations show an irreversible chain growth where N follows a power-law behavior, characteristic of the chaining process in dispersions of superparamagnetic colloids under high external magnetic fields.

- The simulation results are in agreement with the thermodynamic self-assembly theory also presented in this work. The analytical model predicts that the average chain length in the equilibrium state can be described by a dimensionless parameter N^* combining the volume fraction of colloids π_0 and the magnetic coupling parameter Γ. We have also discussed under which experimental conditions this equilibrium state can be observed. We assert that values of Γ in the range 10-15 can be easily obtained in experiments, for instance, using superparamagnetic colloids of 100 nm in size and with a saturation magnetization of 30 emu g^{-1}. We would like to stress here that, after the publication of our work, some *Small Angle X-ray Neutron Scattering* (SANS) experiments were presented, supporting the existence of such an equilibrium state [113].

- In view of the thermodynamical model, we have proposed a new aggregation criterion in the basis of the aggregation parameter. We expect aggregation for $N^* > 1$. This criterion replaces the previous one, which typically assumes that for $\Gamma > 1$ the system is driven by the magnetic interactions rather than by thermal fluctuations, an statement which is not in agreement with our simulations.

- We have introduced an *on-the-fly* Coarse-Grain model to describe the chaining phenomenon observed in dispersions of superparamagnetic colloids under strong magnetic fields. A good agreement with standard LD simulations is found in a wide range of volume fractions and magnetic strength parameter. The implementation of this new Coarse-Grain model presented has been made available free of charge for the scientific community through the web [119]. The software has been registered at the Spanish Intellectual Property Office, registry number G00117-12, affidavit AN6340271.

- The main advantage of the Coarse-Grain methodology presented is its low computational cost in terms of CPU time. With the present Coarse-Grain approach, we were able to correctly predict the time dependence of the transverse relaxation time T_2 of water protons in superparamagnetic colloidal dispersions.

Chapter 3

Results II: Magnetophoresis

In this chapter we present the results corresponding to the separation of superparamagnetic colloidal dispersions using inhomogeneous magnetic fields. The results here summarized have been published in the following articles:

> **Article 3:** "Simple analytical model for the magnetophoretic separation of superparamagnetic dispersions in a uniform magnetic field gradient", *Physical Review E* **84**, 021402 (2011).
>
> **Article 4:** "Simulation of Magnetophoretic processes in dispersions of superparamagnetic nanoparticles in the non-cooperative regime", *Journal of Nanomaterials*, Article ID 678581 (2012).
>
> **Article 5:** "Magnetophoresis of colloidal particles in a dispersion of superparamagnetic particles: theory and experiments", *Soft Matter* **8**, 6039 (2012).

3.1 Objectives

1. Obtain an analytical solution to characterize the *non-cooperative* magnetophoresis separation under homogeneous magnetophoretic conditions.
2. Propose a simple and low-cost simulation technique to study the *non-cooperative* magnetophoresis separation process for different separators and magnetic colloids.
3. Study analytically and by simulations the magnetic separation process in heterogeneous dispersions of magnetic and non-magnetic colloids.

3.2 Summary

Magnetophoresis is a phenomenon of great interest in novel applications involving magnetic nanoparticles and colloids. Among all different applications in which this phenomenon is exploited, we will focus our attention on the magnetic separation. It has been shown that two different magnetic separation regimes exist, named *cooperative* and *non-cooperative* magnetophoresis [52]. These two different regimes have been shown to be related to the aggregation phenomenon typical in superparamagnetic dispersions under large magnetic fields and discussed in section 1.3.3. We have shown that the distinction between these two regimes is due to the formation of chain-like aggregates induced by the magnetic fields applied. In previous chapter, we have provided an aggregation criterion ($N^* > 1$) to evaluate when the formation of such chain-like structures should be expected. We will present simulation and analytical results of the separation process of magnetic colloidal particles, taking advantage of the homogeneous magnetophoretic conditions found in our experimental setup (see section 1.3.3 for more details on the setup), which has proven to provide a more suitable framework to develop analytical tools. Previous theoretical and simulation studies on the magnetic separation have been focused in the individual motion of particles inside the separator or in the quantification of the overall capture rate of the process. Our aim here is to provide theoretical tools (analytical solutions and/or simulation models) to face the cooperative and non-cooperative magnetic separation processes discussed in the introduction. We will also extend our methodologies to other cases of interest, such as mixtures of different colloidal particles, with different size and magnetic response. In addition, we will show by experiments and simulations, how magnetic nanoparticles can be used to tune the magnetic response of latex colloids, inducing different magnetophoretic behaviors. The possibility to adjust the magnetic response of non-magnetic materials by external agents has many advantages among traditional magnetic bead separation strategies and has direct implications in existent technologies.

In this chapter we will summarize the results corresponding to different magnetophoretic separation processes studied. All experiments were conducted by our collaborators Dr. Lluís Miquel Martínez from SEPMAG Tecnologies S.L. and Dr. Maria Benelmekki from University of Minho, Braga (Portugal). In these separation experiments Precision Magnetophoresis Separator devices from SEPMAG Technologies have been used: the SEPMAG LAB 1×25ml 2042 and the SEPMAG LAB 1×25ml 2042 plus, characterized by field gradients of 30 T/m and 60 T/m, respectively [90]. These devices, with cylindrical symmetry along the vertical axis, posses an arrangement of magnets which provides homogeneous magnetophoretic conditions, i.e., the magnetic field gradient points toward the cylindrical vessel wall and it is approximatively uniform across the whole separation volume. A more detailed description of these devices and the monitoring system has been provided in section 1.3.3.

3.3 Results

3.3.1 Magnetophoretic separation under homogeneous conditions

We have analyzed magnetophoretic separation experiments corresponding to different aqueous dispersions of superparamagnetic colloids as provided by our collaborators. In order to describe the separation process under such conditions, we have proposed an analytical model based on a non-interacting particle scheme. For this purpose, it is required that the colloids do not form chains due to the induced magnetic dipole-dipole interaction during the magnetic separation process. In this situation, the fulfillment of the non-aggregation criterion $N^* \ll 1$ discussed in [117] ensures that the separation process corresponds to the non-cooperative case.

For mathematical simplicity, but in good approximation, we have described the particle magnetization by a Langevin response function (Eq. 1.5), typical in theoretical descriptions of superparamagnetism. [1, 8, 11, 49]. The set of particles used in our studies are listed in Tab. 3.1. It is important to notice here that the physical parameters required in our analytical expression are rather simple to obtain by experiments. Despite the approach presented in this work is identical to the one followed by Senyei *et al.* [76], we have extended its validity to the non-linear part of the magnetization response of the particles (i.e for large applied magnetic fields). In Tab. 3.1 we have summarized the size and saturation magnetization of all different samples used in these experiments, as well as the value of the aggregation parameter used to predict the formation of chains under the separation conditions of interest. In the same table, we also show the values of the aggregation parameter N^* obtained for the colloids used in our studies.

If the condition $N^* < 1$ is fulfilled, the velocity of a single particle in the steady state can be obtained by noting that the viscous drag force exerted by the solvent is equal in magnitude to the magnetic force over the particle. Under those assumptions, the magnetophoretic velocity of a single particle at a distance r from the center of the separator can be written as:

$$v(r) = v_s \mathcal{L}[\beta r \;\; L] \tag{3.1}$$

where $\mathcal{L}(x)$ is the Langevin response function and L is the radius of the separator. Additionally, we have defined the parameters v_s and β as:

$$\begin{aligned} v_s &= \frac{2R^2}{9\eta}\mu_0\left(\frac{H}{r}\right)M_s\rho_p & (3.2)\\ \beta &= b\mu_0\left(\frac{H}{r}\right)L & (3.3)\end{aligned}$$

where v_s is the magnetophoretic velocity of the particle at saturation, η is the viscosity of the solvent, H is the external magnetic field applied, M_s is the magnetization per

Table 3.1: Diameter, overall density and magnetic moment for the colloidal particles reported in article 4. The last two columns are the magnetic strength and the aggregation parameter calculated from particle properties under the experimental conditions of interest. This table summarizes the values supplied in article 3, table 1.

Sample	2R [nm]	ρ [g/cm^3]	m$_s$ [J/T]	Γ	N^*
S1 (γ-Fe$_2$O$_3$)	12	4.86	3.0×10^{-19}	2.5	0.1
S2 (γ-Fe$_2$O$_3$@SiO$_2$)	82	2.40	3.0×10^{-18}	0.8	0.02
S3 (γ-Fe$_2$O$_3$@SiO$_2$)	157	2.35	1.7×10^{-17}	3.5	0.2
Estapor® M1-020/50	200	1.10	2.5×10^{-16}	$\sim 10^3$	$\sim 10^{21}$

unit volume at saturation, and ρ_p and R are the density and the radius of the particle, respectively. The dimensionless parameter β can be interpreted as the ratio between the magnetic field at the walls and the typical magnetic field b^{-1} required to bring the particle to magnetic saturation.

From Eq. 3.1 and setting the initial conditions (see section II in article 4 for more details), we can obtain an exact analytical expression for the fraction of particles remaining inside the separator at a given time:

$$t = \frac{L}{\beta v_s} \ln \left[\frac{\beta \cosh(\beta) - \sinh(\beta)}{\beta\sqrt{f}\cosh(\beta\sqrt{f}) - \sinh(\beta\sqrt{f})} \right] \tag{3.4}$$

In other words, Eq. 3.4 it gives the time t needed to reach the state with a fraction of particles f still in solution.

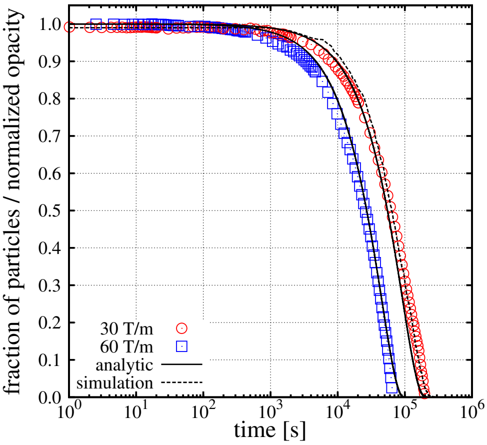

Figure 3.1: Kinetics of magnetophoretic separation of a 10 gL^{-1} dispersion of superparamagnetic γ-Fe$_2$O$_3$ colloids (sample S1). Symbols correspond to the experimental data under 30 T/m (circles) and 60 T/m (squares) and solid lines are the predictions from the analytical model. The dashed line for the 30 T/m case corresponds to the particle tracers simulations. Figure obtained from results presented in articles 3 and 4.

Complementary to this analytical model, we have also designed a 2D simulation scheme based on the Particle Tracers approach. The only difference between the analytical and the simulation model proposed is the accuracy in the description of the magnetic field inside the separator. In simulations, the magnetic field is calculated taking into account the real arrangement of the magnets rather than assuming a uniform magnetic field gradient in the whole volume. The description adopted for the magnetic field in simulations reproduces more accurately the real magnetic field (and magnetic field gradient) than in the analytical model.

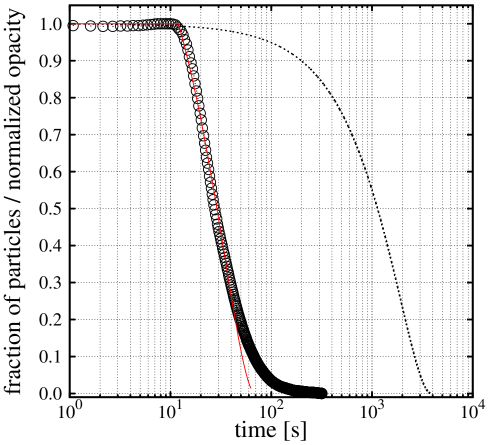

Figure 3.2: Comparison between the experimental results (symbols) obtained from the separation of a 1 gL^{-1} dispersion of commercial Estapor® M1-020/50 particles using the 30 T/m separator and the predictions by the analytical model (dashed line). The velocity of a single particle in saturation has been estimated by using the values presented in Tab. 3.1, giving $v_s \approx 4.0 \times 10^{-6}$ m/s. The solid line (red) is a fit of the initial decay, leaving the magnetophoretic velocity as a fitting parameter. The value for the magnetophoretic velocity obtained from this fit is $v_s \approx 2.6 \times 10^{-4}$ m/s, which greatly exceeds the predicted value for a single colloidal particle. This figure corresponds to figure 3 from article 3.

In Fig. 3.1 we show the experimental results obtained for the S1 sample in two different gradients and their comparison with the analytical model and the simulations (in this last case, we have only presented the case for the 30 T/m gradient). Notice that the obtained agreement between the experiments and both models is remarkably good and the small differences found between the analytical and the simulation results are ascribed to the different accuracy of the magnetic field description in each model. For samples S2 and S3 the matching between theory and experiments is less satisfactory. Despite a more sophisticated modeling of the magnetic response is possible (for instance as proposed in [8]) we preferred to maintain the model as simple as possible, even at the cost of losing some accuracy in the results.

For the commercial sample Estapor® M1-020/50 (γ-Fe_2O_3) we expected high degree of aggregation, since $N^* \gg 1$. In this case, we show that the proposed model is not able to predict the separation kinetics experimentally observed for these colloids (see Fig. 3.2). The large differences between the predicted and the experimental separation time are, in fact, a clear evidence that in this case, the magnetophoretic separation is driven by a different mechanism than the expected from the non-interacting particle model. For instance, the predicted separation time for this sample is about 2 hours in the 30 T/m device, while the experimental separation finished in less than 2 minutes.

Finally just remark that we have also shown that the non-cooperative magnetophoresis separation exhibited by samples S1, S2 and S3 have a universal behavior. The experimental curves obtained in our experiments for those samples can be reasonably collapsed into a single curve after proper rescaling (see figure 4 in article 3).

3.3.2 Separator design

As it was stated in the introduction, in any separation application, one of the key ingredients is the design of efficient magnetic fields. As in previous section, we have employed the same Tracer Simulations approach to investigate different arrangements of magnets in our separation device. More specifically, we have compared the performance of two different separation devices in the non-cooperative magnetophoresis regime. The so-called, *close-type* separator, a category which includes the devices from SEPMAG, and the *open-type* separator, a similar design in which the magnets no longer generate a quadrupolar field, since some magnets are removed with the aim to facilitate the visual contact with the dispersion during the separation process.

From Eq. 1.18, it is straightforward to show that the velocity of a single spherical superparamagnetic colloidal particle in solution can be expressed as:

$$v = \frac{2\mu_0 \rho_p M(H) R_p^2}{9\eta} \quad H \tag{3.5}$$

Then, it is clear that to calculate the velocity of a colloidal particle one needs its basic properties (density, magnetic response and radius), the viscosity η of the medium, and the values of the magnetic field in the separation device.

In article 4 we have compared these two different separator designs, differing only on the arrangement of the magnets (see Fig. 3.3). We have compared the performance of both devices in separating a sample of 10 gL^{-1} of superparamagnetic γ-$\mathrm{Fe_2O_3}$ colloids (corresponding to sample S1 in Tab. 3.1). The fraction of remaining particles in the separator have been computed as a function of time. The faster separation in the close-type separator is due to different factors. On the one hand, in the close-type separator there is a larger amount of particles with higher induced magnetizations than in the open-type. On the other hand, the trajectories followed by the particles in the close-type are shorter than in the open-type. A movie corresponding to both simulations is available on the internet [120]

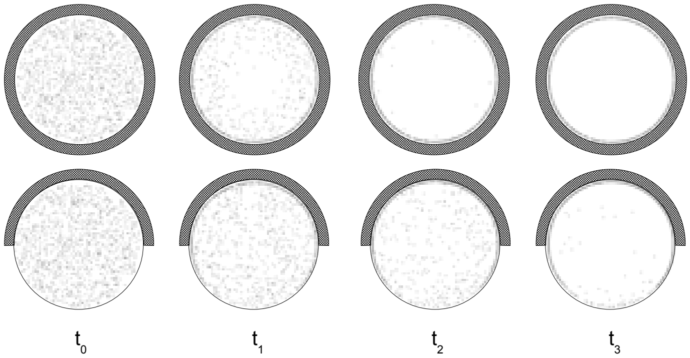

Figure 3.3: Snapshots corresponding to the separation process of a superparamagnetic dispersion of particles (sample S1) at different times ($t_0 = 0$ s, $t_1 = 1 \times 10^5$ s, $t_2 = 2 \times 10^5$ s and $t_3 = 5 \times 10^5$ s). The dark circular areas indicate the location of the magnets. The different figures correspond to simulations in open-type (top row) and close-type (bottom row) geometries, and show how the close-type geometry offers a much more homogeneous and faster separation than the open-type one. The magnetic field and the corresponding magnetic gradient obtained for both configurations are shown in figures 1 and 3 from article 4 and this figure has been adapted from figure 4 from article 4.

3.3.3 Mixtures of magnetic and non-magnetic particles

In this section we will discuss the magnetophoretic behavior of non-magnetic colloids inside a solution of magnetic particles under homogeneous conditions. Such system was inspired by the experiments conducted by our collaborators using a mixture of commercial 900 nm latex colloids immersed in a water solution of 12 nm γ-Fe_2O_3 nanoparticles (sample S1 in Tab. 3.1) with concentration 10 gL^{-1} and using the same SEPMAG separator than in section 3.3.1.

The different steps in the magnetophoresis process were monitored qualitatively with a standard photographic camera, since opacity measurements cannot distinguish between both type of particles in solution. Snapshots of the top view of the mixture at different times obtained with the 60 T/m device are provided in Fig. 3.4. After introducing the mixture in the separator, it was observed that the magnetic nanoparticles started to accumulate at the vessel's wall. Meanwhile, the latex particles (pink/red color) situated near the vessel's wall started moving toward the center of the vessel, while there was also a clear depletion of the latex particles near the center of the separator. After approximatively 6 hours, all the latex particles were concentrated in a ring-shaped structure. Afterwards, this ring-shaped structure started moving toward the vessel's walls (as the nanoparticles did from the start of the process) until they reached the vessel's wall. After their arrival, some remaining magnetic nanoparticles reached the walls, completing the magnetophoresis experiment. A sketch of the different stages observed in the experiment is given in figure 3 from article 5.

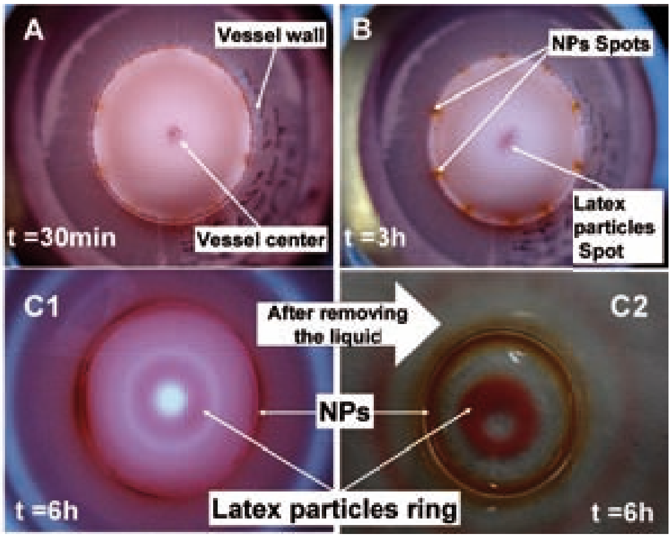

Figure 3.4: Magnetophoretic behavior of a mixture of latex particles (red/pink color) and a SDS-NPs suspension under a 60 T/m gradient. (A) After 30 minutes inside the magnetic system, a red/pink spot appears at the center of the vessel, indicating the beginning of latex particles migration to the center of the bottle. (B) After 3 hours, brown-yellow spots appear close to the walls of the vessel confirming the continuous arrival of the SDS-NPs to the walls and the central red spot size increases slightly. (C1 and C2) After 6 hours, the latex particles ring is formed. A clear depletion of the latex particles both near the walls and also at the center of the system is observed. This picture corresponds to figure 4 from article 5.

In order to predict under which conditions this *go & come back* motion of the latex colloids in the superparamagnetic dispersion is expected, we decided to apply a similar analytical and simulation approach than the employed in the previous section. As we have seen in the introduction (section 1.2.2), the motion of a non-magnetic colloid in a magnetizable medium depends on the mismatch between its magnetization and that of the medium. Thus, one needs to account for the time evolution of the local density of magnetic nanoparticles in order to describe the motion of the latex particles. Hence, as in similar works [67–69], we have adopted the continuum approximation for the solvent, in which the effective magnetization of a colloidal particle immersed in a magnetizable medium is given by Eq. 1.14. Thus, using Eq. 1.14 to calculate the magnetization of a colloidal particle of radius R_c and magnetic moment m_c (in our case, the latex colloids), we can easily write its velocity $\vec{v}_c$ as a function of the velocity of the magnetic nanoparticles $\vec{v}_f$ as:

$$\vec{v}_c(\vec{r}) = \vec{v}_f(\vec{r}) \frac{R_f}{R_c} \left[\frac{m_c}{m_f} - \frac{4}{3}\pi R_c^3 n_f(\vec{r}, t) \right] \tag{3.6}$$

where R_f is the radius of the nanoparticles with magnetic dipole m_f and $n_f(r\ t)$ represents the local concentration of nanoparticles in solution.

Having a look to expression 3.6, one realizes that three possible scenarios arise depending on the mismatch between the magnetization of a colloidal particle and the surrounding fluid. Specifically, these scenarios depend on the ratio $m_c\ m_f$ and on the evolution of $n_f(r\ t)$. If $m_c\ m_f = 0$, the motion of a colloidal particle will be in the direction opposite to the motion of the nanoparticles. In contrast, for large values of $m_c\ m_f$, the colloidal particles will move in the same direction that the superparamagnetic nanoparticles, contrary to the previous situation. Nevertheless, for certain intermediate values of the ratio $m_c\ m_f$, colloidal particles coming from the walls will reverse their motion. Initially, they will move in an opposite direction to the one followed by the superparamagnetic nanoparticles but, at some point, they will reverse their motion and will move in the same direction than the nanoparticles due to decrease of the local concentration of nanoparticles, n_f, in the surroundings of the colloidal particle. Then, in order to describe the motion of the latex colloids in the SEPMAG separator, we have provided an expression for this local concentration of nanoparticles, $n_p(r\ t)$. As a first approximation, at a given instant of time, t, the local concentration of nanoparticles is given approximatively by $n_f(r\ t) = n_{f,0}(1 - v_f t\ r)$ for distances r verifying $r > v_f t$ and $n_f(r\ t) \approx 0$ elsewhere. Here r is the radial coordinate ($r = 0$ at the center of the separator and $r = L$ at the walls), $n_{f,0}$ is the initial uniform concentration and v_f is the velocity of the superparamagnetic nanoparticles at saturation, given by Eq. 3.2. Combining these definitions with Eq. 3.6, we have obtained the differential equations giving the motion of the latex particles (equations 5a and 5b in article 5). These equations can be solved numerically to obtain the trajectory $r(t)$ for a latex particle initially at the walls of the separator. Thus, solving these equations for different values of the ratio $m_c\ m_f$, we have estimated the time required for the latex particles to form the ring-shaped structure, T_r, and the separation time, T_c, for the ring to reach the walls. Some calculated values have been shown in table 1 from article 5. Comparing the experimental times (for the ring formation and separation) with the predicted ones by the theoretical model, we have estimated that in our experiment the ratio is approximately $m_c\ m_f \sim 500$.

Complementary to this results, we also performed Particle Tracer simulations of the system by computing the trajectories of both type of particles using Eq. 3.5 to describe the superparamagnetic nanoparticles motion and Eq. 3.6 for the latex particles one. There are two main differences between these simulations and our analytical model. First, in the simulations, the magnetic field (and gradient) is calculated as the sum of he contributions of each individual magnet in the device, rather than assuming a constant and radial magnetic field gradient. Second, the local density of magnetic nanoparticles surrounding each latex particle, n_f, has been calculated from the positions of the nanoparticles during the simulation. The results obtained from simulations (ring formation and separation time) using the ratio $m_c\ m_f = 500$ were also in good agreement with experimental evidences. Snapshots of the 2D simulations showing the different stages in the separation process are given in Fig. 3.5.

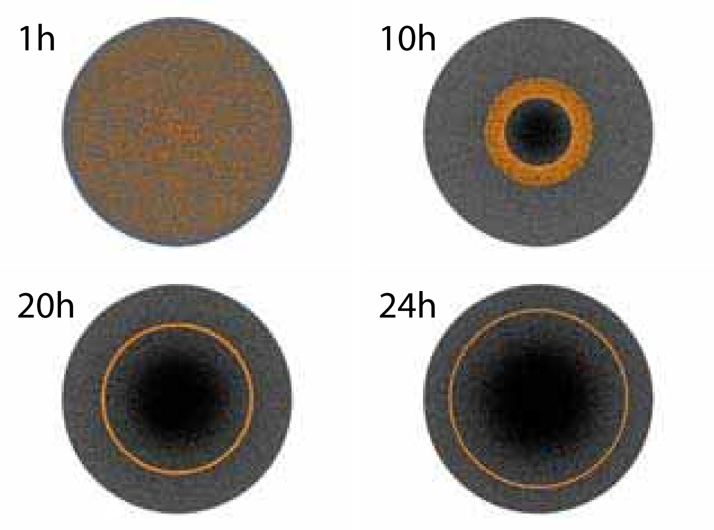

Figure 3.5: Snapshots from the 2D-simulations of the magnetophoresis of an aqueous dispersion of γ-Fe_2O_3 superparamagnetic nanoparticles (grey) and latex polystyrene particles (orange) under a magnetic gradient of 30 T/m at different times. Original snapshots in figure 6 from article 4.

Since the commercial latex particles are not intrinsically magnetic, and in view of the behavior observed in the experiments (corroborated by the calculations and simulations performed with our models), we pointed out that some superparamagnetic nanoparticles may be adsorbed onto the surface of the latex particles. In order to experimentally confirm the adsorption of NPs onto the surface of the latex particles, our collaborators conducted different *Scanning Electron Microscopy* SEM, *Energy Dispersive Spectometer* (EDS) and *Electrophoretic Mobility* from a sample of latex particles obtained from the ring structure formed after 6 hours (Fig. 3.4 C1). Those experiments conclude that the amount of adsorbed nanoparticles per latex colloid was in the range $400 - 3000$, in agreement with our calculations. The results obtained by those techniques were appended as part of the supplementary information of the original article.

3.4 Conclusions

- We have presented an analytical model for the description of the non-cooperative magnetophoretic separation under homogeneous conditions i.e. a uniform magnetic field across the whole separation volume. The results have been compared against real experiments of superparamagnetic colloids with different sizes and magnetizations, as well as under different magnetic field strengths. The expressions obtained are valid under certain restrictive but realistic conditions, which have also been discussed.

- Our analytical results have also shown the existence of a universal curve, onto which experimental results obtained for different colloids should collapse after proper rescaling, provided that they correspond to the non-cooperative separation regime.

- We have presented a low-cost simulation strategy based on the concept of Particle Tracers simulations and applicable to the non-cooperative magnetophoretic separation. This simulation approach was validated by comparing the results obtained against existing experimental and analytical results obtained for the magnetic separation of γ-Fe_2O_3 superparamagnetic nanoparticles.

- We have shown that the homogeneous magnetophoretic conditions created by a close-type separator with quadrupolar field geometry improve the separation process, providing a better control of the separation and reducing the separation time when compared to similar open-type designs.

- We have shown how the motion of non-magnetic particles can be controlled by employing a suspension of superparamagnetic nanoparticles to indirectly tune the magnetic response of the colloidal particles. We have focused our attention in the homogeneous magnetophoresis separation process, already presented in previous works, providing an analytical solution to the kinetics of these systems in a rather simple way.

- We have also extended the simulation strategy to mixtures of colloidal particles immersed in superparamagnetic dispersions. We were able to successfully describe the kinetics of such mixtures observed in experiments.

- Regarding the mixtures of magnetic and non-magnetic colloids, we have found three different scenarios depending on the magnetic response of the particles. The experiments reported here have shown a *go & come back* motion of latex particles in a suspension of superparamagnetic NPs. To explain these observations, we have suggested the adsorption of NPs at the surface of the latex colloids. The estimated amount of NPs adsorbed by the theoretical models has been confirmed by three independent experimental techniques: SEM, EDS and electrophoresis.

Chapter 4

Conclusions & Perspectives

Along this manuscript, we have presented different computer simulations results, analytical models and experiments of superparamagnetic colloidal dispersions. Our attention has been focused in the study of two main issues: the aggregation phenomena observed in superparamagnetic dispersions under external magnetic fields and the magnetic separation of particles in such dispersions by using inhomogeneous magnetic fields. We have discussed the underlying physics arising in such systems in sight of the results obtained, providing new descriptions and simulation approaches to face some concrete problems of special scientific relevance and also of interest in real applications. Here we summarize the main conclusions derived from this work.

4.1 Conclusions

The first part of our results, presented in Chapter 2, has been devoted to investigate the aggregation kinetics of superparamagnetic colloids under homogeneous external magnetic fields, and the main conclusions of this work can be summarized as follows:

- We have shown by Langevin Dynamics simulations the existence of different kinetic aggregation regimes arising in superparamagnetic dispersions. The simulations have shown the existence of an equilibrium state, which can be experimentally accessed for certain values of volume fraction of colloids and magnetic strength. This is the first time that the existence of such an equilibrium state is reported on the basis of computer simulations. We have also shown that in other situations, the aggregation kinetics follows a power-law behavior typical to irreversible aggregation processes and the values for the kinetic exponents here reported are in agreement with previously reported kinetic exponents for similar systems.
- We have presented a theoretical model based on a thermodynamic self-assembly theory, which supports the existence of such an equilibrium state. According

to this model, the equilibrium state is defined by the dimensionless aggregation parameter, N^*, which depends on the volume fraction of colloids π_0 and the magnetic strength parameter Γ. The model provides a criterion to predict the formation of chain-like structures in superparamagnetic dispersions based on these parameters, as well as the equilibrium values expected for the average chain length in equilibrium. The predictions of the model show a good agreement with results obtained by Langevin Dynamics simulations.

- On the basis of a coarse-grain approach, we have presented a new simulation model intended to face experimental problems which were unaffordable by Langevin Dynamics simulations. The new methodology is designed to reproduce the irreversible chain growth kinetics (already observed by using Langevin Dynamics) at larger timescales. The simulation results obtained with the new model are in agreement with Langevin Dynamics simulations and have been used to explain the time evolution experimentally found in the T_2 relaxation time of water protons in superparamagnetic dispersions.

In the second part of our study, summarized in Chapter 3, we have focused our attention on the controlled magnetophoretic motion of colloidal particles. More specifically, we have investigated the underlying physics in the magnetic separation process of superparamagnetic particles under uniform field gradients. The conclusions derived from these investigations are listed below:

- We have formulated an analytical model to describe the non-cooperative magnetic separation process under certain homogeneous conditions. The particles are described by a rather simple model, in which only the radius of the particles, their density and their magnetic response are required. We have shown how this model suffices to reproduce the non-cooperative magnetic separation results obtained for different type of particles, from nanometer crystalline particles to more complex composite structures.

- A rather low-cost simulation strategy, based on Particle Tracers simulations, has been presented as a complementary tool to analyze the separation process. This approach has also provided a framework to analyze the performance of different magnetic separator designs, and has helped to elucidate different key factors in these separators.

- An extension of the analytical and simulation approaches previously mentioned has allowed the study of the controlled motion of latex colloidal particles in superparamagnetic dispersions. The complex motion exhibited in experiments by the latex particles has been explained in view of the theoretical model proposed, together with Particle Tracer simulations.

4.2 Perspectives

Nevertheless, some questions about those systems are still open problems of interest for different reasons, either from the theoretical point of view or from their implications in real applications [121]. Here we point out some questions that could be addressed as a natural extension of the research conducted along this thesis:

1. One important problem of interest in many applications is the separation of different types of particles from the same sample. Nowadays, several approaches have been proposed in order to separate different magnetic particles in solution, most of them based on differences in size and/or magnetic response. We envisage a different approach to the fractionation of particles, based on the different magnetophoretic separation regimes (cooperative *vs.* non-cooperative) exhibited by superparamagnetic nanoparticles. As we have seen, the cooperative separation is much faster than the non-cooperative one. Then, one strategy would be to promote the fast separation regime of the target particles leaving the other particles separate under a non-cooperative regime. To this end, one would be interested in inducing the formation of chains of target particles while letting any other particle in solution out of the chain-like structures.

   As example of this approach, we have examined by Langevin Dynamics simulations mixtures of -Fe_2O_3 ($\Gamma \approx 34$) and α-Fe_2O_3 ($\Gamma \approx 0\ 2$) particles (typical products in some synthesis routes of iron oxides magnetic particles [122]). Preliminar results agree with our predictions. As we expected from the magnetic strength parameters estimated for these particles, we have found that -Fe_2O_3 particles form chain-like structures while α-Fe_2O_3 particles remain as single colloids in solution. After 10s, the average chain length formed by -Fe_2O_3 particles is $N \approx 15$, while no particle of type α-Fe_2O_3 is found in any of the chains formed.

   This new fractionation approach would help in purification of superparamagnetic colloids, since the large difference in separation times expected from both regimes would enhance the separation window.

2. Along our research, we have focused the attention on the chaining process in superparamagnetic dispersions. Nevertheless, it is known that, under certain circumstances, the chains coalesce into larger bundle-like structures. This phenomenon has been previously reported in different experiments, and recent *Nuclear Magnetic Resonance* (NMR) experiments and Molecular Dynamics simulations have shown that both processes (chaining and bundling) seem to occur at very different timescales [73]. It is proposed that the bundling process happens once a substantial amount of chains are already present in solution. Thus, a natural extension would be the study of this bundling process by Langevin Dynamics simulations, with the aim to elucidate the key factors driving the lateral coalescence of superparamagnetic chains and the kinetics of the process. In view of these results, one could then extend the proposed Coarse-Grain model in order to include this new observed aggregation phenomenon, which operates at timescales

different from the chaining process studied here.

3. Another intriguing problem is the fast magnetic separation observed in the cooperative regime [52] and intimately related to the formation of different colloidal structures due to the application of a magnetic field. Under some conditions, these systems will mainly contain chain-like structures, and the formation of more complex structures during the separation will appear as a result of other mechanism like, for instance, lateral collisions between chains due to their different velocities. One could easily extend the model implemented in the MAGCHAIN code to tackle the description of the cooperative magnetophoresis separation by supplying an aggregation criterion to account for the lateral coalescence of chains by these other mechanisms. This extension of the model would help to shed some light in the fundamental physical laws of the cooperative magnetic separation process and its kinetics.

4. The aforementioned model implemented in the MAGCHAIN code could also be extended to account for the disaggregation of chain-like structures. The aim of this extension would be to describe systems for which one expect to find an equilibrium state at larger times, a situation unaffordable by Langevin Dynamics simulations. Thanks to the low CPU cost of this simulation methodology, one would be able to systematic study this equilibrium state (as predicted by the thermodynamical model here presented). This extension would extend the applicability of the MAGCHAIN code to address the magnetic separation of superparamagnetic dispersions in different situations.